Cell Metabolism

Article

Adenosine/A2B Receptor Signaling Ameliorates the Effects of Aging and Counteracts Obesity

Graphical Abstract

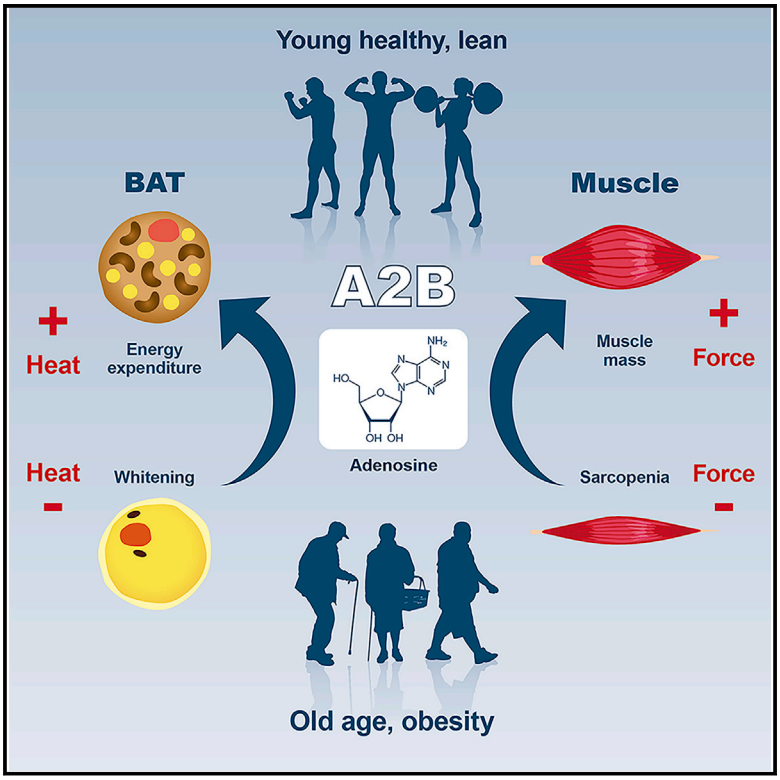

Authors

Thorsten Gnad, Gemma Navarro, Minna Lahesmaa, ..., Wilhelm Bloch, Kirsi A. Virtanen, Alexander Pfeifer

Correspondence

alexander.pfeifer@uni-bonn.de

In Brief

Gnad et al. demonstrate that the adenosine A2B receptor is expressed by and regulates two major energy dissipating tissues: skeletal muscle and brown fat. Moreover, pharmacological activation of this receptor restores and maintains the function of these tissues during aging and obesity.

Highlights

- A2B receptor regulates two major energy dissipating tissues: muscle and brown fat
- Activation of A2B counteracts sarcopenia as well as obesity in mice
- A2B forms heteromers that are crucial for physiological adenosine signaling
- A2B expression correlates with energy expenditure in human muscle and brown fat

Gnad et al., 2020, Cell Metabolism *32*, 56–70
July 7, 2020
https://doi.org/10.1016/j.cmet.2020.06.006

CellPress

CellPress

Cell Metabolism

Article

Adenosine/A2B Receptor Signaling Ameliorates the Effects of Aging and Counteracts Obesity

Thorsten Gnad,[1] Gemma Navarro,[2,3] Minna Lahesmaa,[4] Laia Reverte-Salisa,[1] Francesca Copperi,[1] Arnau Cordomi,[5] Jennifer Naumann,[1] Aileen Hochhäuser,[1] Saskia Haufs-Brusberg,[1] Daniela Wenzel,[6,7] Frank Suhr,[8,9] Naja Zenius Jespersen,[10] Camilla Scheele,[10,11] Volodymyr Tsvilovskyy,[12] Christian Brinkmann,[13] Joern Rittweger,[14] Christian Dani,[15] Mathias Kranz,[16] Winnie Deuther-Conrad,[16] Holger K. Eltzschig,[17] Tarja Niemi,[18] Markku Taittonen,[19] Peter Brust,[16] Pirjo Nuutila,[4] Leonardo Pardo,[5] Bernd K. Fleischmann,[6] Matthias Blüher,[20] Rafael Franco,[2,3] Wilhelm Bloch,[8] Kirsi A. Virtanen,[4,21] and Alexander Pfeifer[1,22,*]

[1]Institute of Pharmacology and Toxicology, University Hospital, University of Bonn, 53127 Bonn, Germany
[2]Department of Biochemistry and Molecular Biomedicine, Faculty of Biology, University of Barcelona, Barcelona, Spain
[3]Centro de Investigación en Red, Enfermedades Neurodegenerativas (CiberNed), Instituto de Salud Carlos III, Madrid, Spain
[4]Turku PET Centre, Turku University Hospital, University of Turku, Turku, Finland
[5]Laboratory of Computational Medicine, Universitat Autonoma de Barcelona, Barcelona, Spain
[6]Institute of Physiology I, Life&Brain Center, Medical Faculty, University of Bonn, 53105 Bonn, Germany
[7]Department of Systems Physiology, Medical Faculty, Ruhr University Bochum, Bochum, Germany
[8]Molecular and Cellular Sport Medicine, German Sport University Cologne, Cologne, Germany
[9]Exercise Physiology Research Group, Biomedical Sciences Group, KU Leuven, Leuven, Belgium
[10]Centre for Physical Activity Research, Rigshospitalet, University of Copenhagen, Copenhagen, Denmark
[11]Novo Nordisk Foundation Center for Basic Metabolic Research, Faculty of Health and Medical Sciences, University of Copenhagen, Copenhagen, Denmark
[12]Institute of Pharmacology, Ruprecht-Karls University, Heidelberg, Germany
[13]Department of Preventive and Rehabilitative Sport Medicine, German Sport University Cologne, Cologne, Germany
[14]Department of Muscle and Bone Metabolism, German Aerospace Center (DLR), Institute of Aerospace Medicine, Cologne, Germany
[15]Université Côte d'Azur, CNRS, Inserm, iBV, Faculté de Médecine, 06107 Nice Cedex 2, France
[16]Helmholtz-Zentrum Dresden – Rossendorf, Institute of Radiopharmaceutical Cancer Research, Research Site Leipzig, Leipzig, Germany
[17]Department of Anesthesiology, University of Texas Health Science Center at Houston, McGovern Medical School, Houston, TX, USA
[18]Department of Plastic and General Surgery, Turku University Hospital, Turku, Finland
[19]Department of Anesthesiology, Turku University Hospital, Turku, Finland
[20]Department of Medicine, University of Leipzig, Leipzig, Germany
[21]Institute of Public Health and Clinical Nutrition, University of Eastern Finland (UEF), Kuopio, Finland
[22]Lead Contact
*Correspondence: alexander.pfeifer@uni-bonn.de
https://doi.org/10.1016/j.cmet.2020.06.006

SUMMARY

The combination of aging populations with the obesity pandemic results in an alarming rise in non-communicable diseases. Here, we show that the enigmatic adenosine A2B receptor (A2B) is abundantly expressed in skeletal muscle (SKM) as well as brown adipose tissue (BAT) and might be targeted to counteract age-related muscle atrophy (sarcopenia) as well as obesity. Mice with SKM-specific deletion of A2B exhibited sarcopenia, diminished muscle strength, and reduced energy expenditure (EE), whereas pharmacological A2B activation counteracted these processes. Adipose tissue-specific ablation of A2B exacerbated age-related processes and reduced BAT EE, whereas A2B stimulation ameliorated obesity. In humans, A2B expression correlated with EE in SKM, BAT activity, and abundance of thermogenic adipocytes in white fat. Moreover,

Context and Significance

In both aging and obesity, the function of muscle and brown adipose tissue declines, predisposing humans to frailty and metabolic disorder. Here, researchers in Bonn, Germany, and their colleagues show that adenosine, a metabolite and signaling molecule, can improve muscle function and brown fat during aging and obesity. Importantly, they find that a synthetic molecule that specifically activates the adenosine "A2B" receptor restores the function of muscle and brown fat in aged and obese mice to the levels of young, lean mice. This work establishes that activation of a single receptor/pathway (i.e., the adenosine/A2B pathway) has the potential to induce healthy aging and to tackle metabolic disease.

A2B agonist treatment increased EE from human adipocytes, myocytes, and muscle explants. Mechanistically, A2B forms heterodimers required for adenosine signaling. Overall, adenosine/A2B signaling links muscle and BAT and has both anti-aging and anti–obesity potential.

INTRODUCTION

Aging and metabolism are closely linked (Barzilai et al., 2012): aging is associated with metabolic decline, whereas metabolic interventions (i.e., caloric restriction) can delay age-related processes and expand life expectancy (Masoro, 2005). A major health issue in the elderly is the loss of skeletal muscle (SKM) mass and strength, a process termed sarcopenia (Sayer et al., 2008). Sarcopenia has important metabolic consequences: SKM is not only responsible for energy expenditure (EE) during physical activity but also contributes largely to EE at rest. Consequently, reduced muscle function can lead to an imbalance in energy homeostasis and obesity (Batsis and Villareal, 2018). Thus, aging is associated with an increase in obesity (Jura and Kozak, 2016), and the prevalence of obesity in combination with sarcopenia (i.e., sarcopenic obesity) (Batsis and Villareal, 2018) is rising in adults aged 65 years and older. Sarcopenic obesity is a high-risk geriatric syndrome associated with frailty, immobility, and increased mortality (Batsis and Villareal, 2018). These two trends—aging populations and obesity pandemic—are per se enormous burden for human health; however, since they are developing increasingly in parallel, they are becoming major threats to the health of ever more individuals and the health systems.

Here, we set out to identify signaling pathways that might be used to ameliorate aging processes and metabolic diseases. Given the importance of cAMP signaling for both SKM and adipocyte function, we focused on G protein-coupled receptors (GPCRs) signaling via G_s protein. In addition, GPCRs have high medical relevance because they constitute the major target of currently available drugs (Hauser et al., 2017). Since systemic stimulation of cAMP signaling via beta2- and beta3-adrenergic receptors (beta2- and beta3-AR) is associated with significant cardiovascular side effects including hypertension and atherosclerosis (Cypess et al., 2015; Sui et al., 2019), the identification of alternative pathways is not only of biological interest, but also has translational potential.

In this study, we focus on the adenosine A2B receptor because we found that this receptor is the most highly expressed G_s-coupled GPCR common to both BAT and SKM. Previous studies of our lab and others (Gnad et al., 2014; Ruan et al., 2018) have shown that the extracellular nucleoside adenosine plays an important role in BAT and that the adenosine A2A receptor directly activates EE (Gnad et al., 2014) as well as induces release of the "batokine" FGF21 (Ruan et al., 2018). However, the function of the other G_s-coupled adenosine receptor A2B in BAT and SKM was enigmatic. Strikingly, we show that specific ablation of A2B in SKM and BAT recapitulated important aspects of aging including reduced muscle strength and mass as well as reduced BAT-dependent EE and "whitening," respectively. In contrast, stimulation of A2B counteracted aging effects in SKM and BAT. Moreover, A2B increased EE and reduced diet-induced obesity (DIO), which was unexpected in the light of BAT activation via A2A. Therefore, we set out to identify the mechanisms of A2B signaling and found that these two G_s-coupled GPCRs form heterodimers that are functionally required for adenosine-mediated activation of BAT. In humans, A2B stimulation increased EE from both primary myocytes and muscle explants. Overall, this study offers not only mechanistic insight into adenosine receptor interaction and A2B function but also how aging and metabolic disease are linked and might be tackled by addressing a single GPCR.

RESULTS

Adenosine Receptor A2B Signaling in SKM

Analysis of G_s-coupled GPCRs in murine SKM and BAT revealed that A2B is abundantly expressed in both tissues (Figure 1A; Table S1). Compared to other tissues, A2B was also most highly expressed in SKM and BAT (Figure S1A). Adenosine is an extracellular signaling molecule regulating tissue physiology by signaling via four different adenosine receptors (AdoRs): A1 and A3, which are G_i-coupled, and A2A and A2B, which are G_s-coupled and stimulate cAMP production. Interestingly, contracting SKM tissue and activated BAT have both been shown to release adenosine (Gnad et al., 2014; Hellsten et al., 1998). On a cellular level, A2B was by far the most highly expressed adenosine receptor in murine C2C12 SKM cells (Figure S1B). Adenosine-induced intracellular cAMP production of C2C12 cells was abrogated by blocking A2B with the specific A2B antagonist PSB603 (Figure 1B), indicating that this AdoR is of high relevance for adenosine signaling in SKM.

To analyze the role of A2B in SKM *in vivo*, we generated SKM-specific A2B knockout mice (SKMA2B-KO) (Figure S1A; Table S2) and found reduced muscle mass compared to control mice (Con-A2B) (Figure 1C). In contrast, stimulation of A2B in wild-type mice with the highly specific A2B agonist Bay 60-6583 (Eckle et al., 2007) significantly increased muscle mass (Figure 1D) and lean mass (Figure S1C). Aging results in a reduction in muscle strength, which is predictive of physical disability in older people (Rantanen et al., 1999). We measured forelimb grip strength, which is a readout for aging-associated physiological decline of SKM *in vivo* (Takeshita et al., 2017), and found 10% reduced strength in young SKMA2B-KO mice. In aged SKMA2B-KO animals, grip strength was decreased by 18% compared to control mice (Figure 1E). In contrast, treatment of wild-type mice with A2B agonist completely restored grip strength to levels of young control mice (Figure 1F). Furthermore, specific muscle force (mN/mm^2) measured in isolated SKM of young SKMA2B-KO was significantly reduced by 26% (Figure 1G), while age-related decline of specific force was further augmented in SKM explants deficient in A2B (Figure 1G). In contrast, treatment of 2-month-old wild-type mice with A2B agonist significantly increased specific muscle force by 15% (Figure 1H). Although muscle force declined during aging, A2B activation significantly increased muscle force by 16% and 24% in 14- and 20-month-old wild-type mice, respectively, reaching levels of young control mice (Figure 1H). Importantly, pharmacological A2B stimulation had no effect on muscle mass and specific force of A2B-deficient mice, showing the

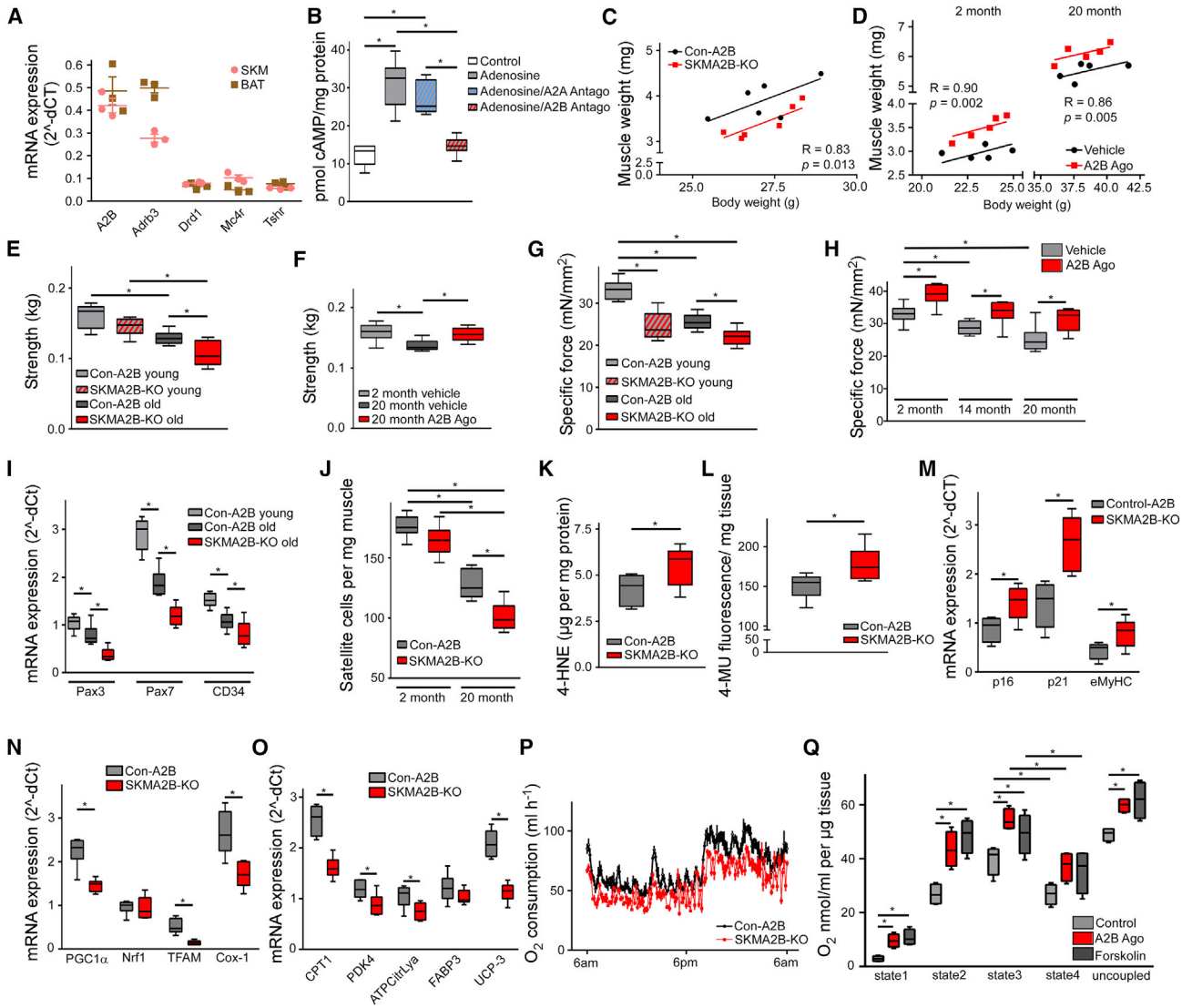

Figure 1. A2B Signaling in Skeletal Muscle

(A) GPCR mRNA expression in murine BAT and SKM (abbreviations in Table S10; n = 3).

(B) cAMP levels in C2C12 pre-treated with A2A (MSX-2; 300 μM) or A2B (PSB603; 150 nM) antagonist prior to adenosine (1 μM) stimulation (n = 6).

(C and D) ANCOVA of SKM/body weight of SKMA2B-KO and Con-A2B mice (C) or mice treated with A2B agonist for 4 weeks (D) (n = 6).

(E and F) Forelimb grip strength of young (2 month) and old (16 month) SKMA2B-KO and Con-A2B (E) or aged mice treated with A2B agonist (F).

(G and H) Specific force of SKM explants from SKMA2B-KO and Con-A2B mice (G) or mice treated with A2B agonist for 4 weeks (H) (n = 6).

(I) mRNA abundance of satellite marker genes in SKM of SKMA2B-KO and Con-A2B mice (n = 5).

(J) Satellite cells in SKM of SKMA2B-KO and Con-A2B mice (n = 6).

(K) 4-hydroxynonenal (4-HNE) in SKM of SKMA2B-KO and Con-A2B mice (n = 8).

(L) Senescence-associated beta-galactosidase activity in SKM of SKMA2B-KO and Con-A2B mice (n = 6).

(M–O) Expression of senescence (M), mitochondrial (N), and oxidative metabolism marker genes (O) in SKM of SKMA2B-KO and Con-A2B mice (n = 6).

(P) Oxygen consumption over 24 h at 23°C of SKMA2B-KO and Con-A2B mice (n = 6).

(Q) Oxygen consumption of SKM explants acutely treated with A2B agonist (300 nM) or Forskolin (1 μM) (state 1, endogenous; state 2, ADP; state 3, succinate; state 4, oligomycin; uncoupled, FCCP; n = 6).

*p < 0.05. Data are shown as mean + SEM (A and P), scatterplot (C and D), or boxplot (with median) and whiskers (1.5× interquartile range) (B, E–O, and Q) and analyzed using two-tailed Student's t test (K–O), ANCOVA (C and D), or ANOVA with Newman-Keuls post hoc test (B, E–J, and Q).

See also Figure S1.

specificity of the agonist used for our experiments (Figures S1D and S1E).

An important hallmark of sarcopenia is declining regenerative capacity of SKM (García-Prat and Muñoz-Cánoves, 2017). Muscle regeneration requires muscle-specific stem cells termed satellite cells (García-Prat and Muñoz-Cánoves, 2017). Analysis of satellite marker genes revealed significantly decreased expression of Pax3, Pax7, and CD34 in muscle of aged SKMA2B-KO

mice compared to control mice (Figure 1I). Vice versa, A2B stimulation of aged wild-type mice significantly increased satellite marker gene expression (Figure S1F). Consequently, satellite cell number was significantly reduced in old SKMA2B-KO mice compared to Con-A2B (Figure 1J) but significantly elevated in aged wild-type mice stimulated with an A2B agonist (Figure S1G). Of note, isolated satellite cells abundantly express A2B compared to other adenosine receptors (Figure S1H). Aging and senescence (i.e., gradual deterioration of tissue function) of SKM are related to the accumulation of oxidized lipids (Marzani et al., 2005), and lipoperoxide plasma levels positively correlate with frailty in humans (Inglés et al., 2014). Analysis of lipoperoxide abundance in SKM showed significantly elevated 4-hydroxynonenal levels—a product of cellular lipid peroxidation—in aged SKMA2B-KO compared to Con-A2B (Figure 1K), while SKM from 20-month-old wild-type mice treated with A2B agonist contained significantly less lipoperoxide (Figure S1I). Moreover, activity of senescence-associated beta-galactosidase (SA-BetaGal)—a functional readout of senescence (Keyes et al., 2005)—was significantly increased in SKM deficient for A2B (Figure 1L). In contrast, stimulation of A2B significantly reduced SA-BetaGal activity in SKM of aged wild-type mice (Figure S1J). Further analysis revealed that marker genes of senescence (p16, p21, and eMyHC) (Sousa-Victor et al., 2014) were significantly upregulated in aged SKMA2B-KO (Figure 1M), but significantly reduced in 20-month-old wild-type mice treated with A2B agonist (Figure S1K).

Mammalian SKM consists of different fiber types: myosin heavy chain (MyHC) isoforms IIb and IIx are expressed in glycolytic fibers, while MyHCI and MyHCIIa fibers have oxidative and mixed properties, respectively (Ferraro et al., 2016; Schiaffino and Reggiani, 2011). Fiber type expression analysis of SKMA2B-KO muscle revealed significantly decreased MyHCIIa and IIb expression (Figure S1L), whereas A2B treatment significantly increased expression of MyHCIIa and IIb by 123% and 151%, respectively (Figure S1M). In line with these data, we found increased staining for type IIa and IIb isoforms after histological analysis of SKM sections from A2B-treated wild-type mice (Figure S1N). SKM is rich in mitochondria and oxidative metabolism is an important determinant of muscle function and energy consumption (Zierath and Wallberg-Henriksson, 2015). There is evidence that mitochondrial function and metabolic supply are impaired in aged muscle (Gouspillou et al., 2014). A2B-deficient SKM showed significantly downregulated expression of genes involved in mitochondrial biogenesis and function (PGC1α, Nrf1, Tfam, and Cox-1) (Figure 1N), in oxidative metabolism (Cpt1, Pdk4, ATP citrate lyase, Fabp3, and UCP-3) (Figure 1O), as well as in differentiation and contractile apparatus (MyoD, Mef2c, and alpha1-actin) (Figure S1O), whereas pharmacological A2B stimulation had the opposite effects (Figures S1P–S1R). These A2B effects in SKM tissue were mirrored in C2C12 myocytes (Figures S1S and S1T).

Analysis of whole-body EE revealed significantly decreased oxygen consumption in SKMA2B-KO (Figures 1P and S1U), whereas acute A2B stimulation significantly elevated EE of wild-type SKM explants (Figure 1Q) and *in vitro* (Figure S1V).

Together, these data show that A2B plays a major role in SKM maintenance and function. A2B deficiency promotes senescence and aggravates aging of SKM, leading to decreased muscle strength and mass as well as reduced EE of aging muscle. Importantly, A2B stimulation counteracts four hallmarks of sarcopenia: loss of muscle function and mass, increased senescence, and declining regenerative capacity. Additionally, A2B activation enhances resting oxidative metabolism and EE in muscle.

A2B Signaling in BAT Activation and Aging

Adenosine has been previously shown to activate murine and human BAT (Gnad et al., 2014). Since not much was known about the role of A2B in BAT, we studied the function of this G_s-coupled receptor in thermogenic adipose tissues. Moreover, BAT shares several features with SKM and contributes to systemic basal metabolism by virtue of its high EE capacity (Enerbäck, 2010; Kajimura et al., 2015; Nedergaard et al., 2011). BAT abundance in human adults inversely correlates with BMI (van Marken Lichtenbelt et al., 2009); however, human BAT function decreases during aging (Cypess et al., 2009).

To test the relevance of A2B for BAT function and in age-related processes, we generated adipose tissue-specific A2B knockout mice (ATA2B-KO) (Figure S2A), which exhibited no significant difference in basic metabolic parameters (Table S3) compared to control mice (Con-A2B). Initially, we studied the role of A2B for physiological BAT-dependent EE. BAT activity in ATA2B-KO newborn mice was significantly decreased as measured by infrared thermography (Figure 2A) compared to Con-A2B animals. Moreover, whole-body oxygen consumption was significantly reduced by 31% in adult ATA2B-KO compared to Con-A2B mice after cold exposure (Figures 2B and S2B), while EE was similar between the two genotypes at thermo-neutrality (Figures S2C and S2D). Conversely, pharmacological stimulation of A2B significantly increased uptake of 2-deoxy-2-[^{18}F]-fluoro-D-glucose ([^{18}F]FDG), the "gold standard" for BAT quantitation, into BAT (Figures 2C and 2D). Oxygen consumption was increased 3-fold by A2B activation in wild-type mice, but no effect of the A2B agonist was observed in A2B-deficient mice (Figures S2E and S2F) or after blockade of A2B signaling with the specific A2B antagonist PSB603 (1 mg/kg) (Figures S2G and S2H), demonstrating again the specificity of the A2B agonist. Moreover, acute pharmacological blockade of A2B prior to cold exposure significantly reduced oxygen consumption by 43% (Figure S2I). Together, these data show that A2B is crucial for physiological BAT activation and BAT-mediated EE can be induced via A2B stimulation.

BAT abundance decreases and negatively correlates with BMI, especially in older subjects, indicating a protective role of human BAT against age-associated obesity (Cypess et al., 2009). Hence, we analyzed aging marker genes sirtuins (Sirt1 and Sirt3) and Forkhead box protein A3 (Foxa3), which are down- and upregulated in aging, respectively (Brown et al., 2013; Ma et al., 2014). In A2B-deficient murine BAT, we found significantly decreased levels of Sirt1 and Sirt3 (Figure 2E). Foxa3 levels are increased in BAT during aging, and in BAT of ATA2B-KO, Foxa3 was significantly upregulated (Figure 2E). Markers of cellular senescence Caveolin1, Activin A, p16, and p21 were significantly upregulated in the absence of A2B (Figure 2E). Age-induced oxidative stress impairs adipogenesis and thermogenesis in brown fat (Cui et al., 2019). Levels of

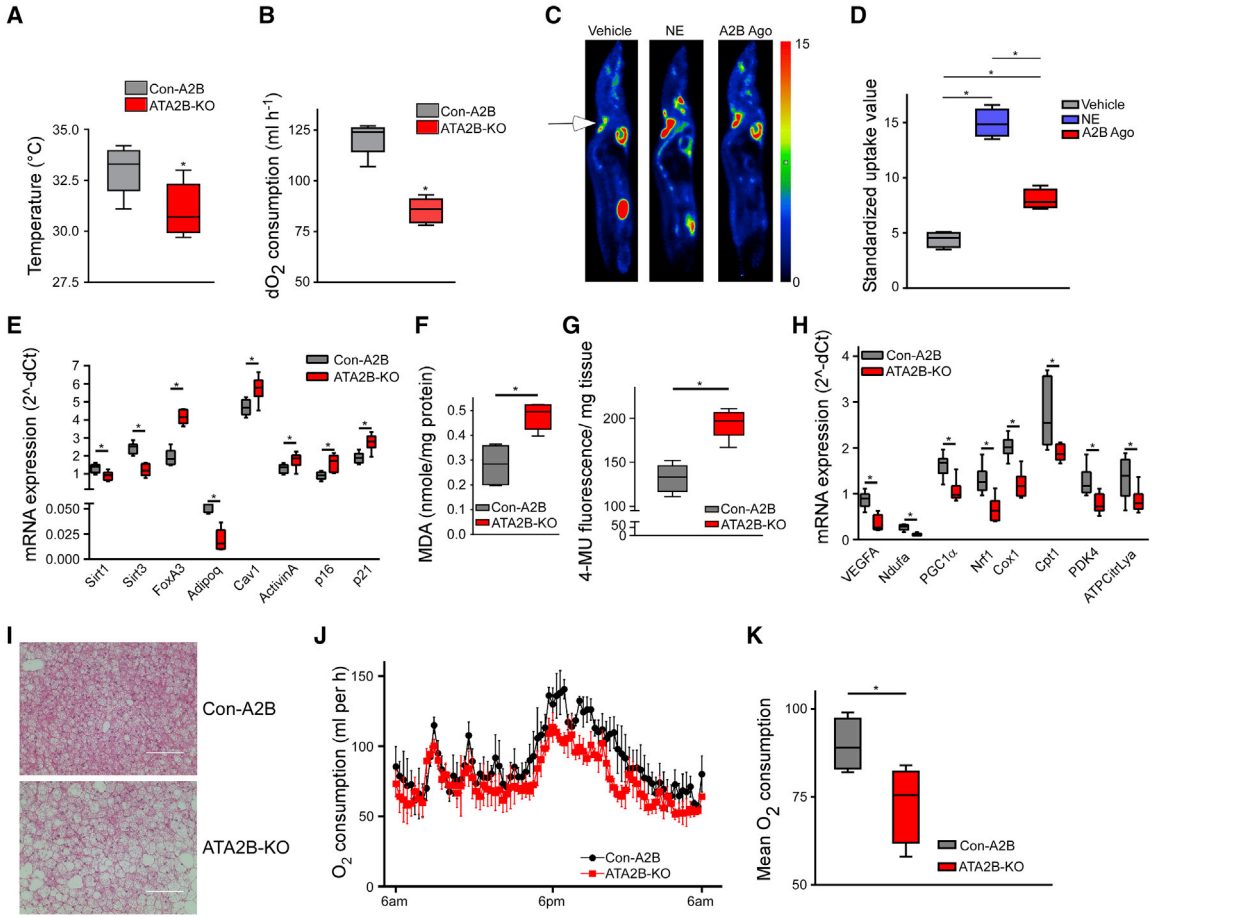

Figure 2. The Role of A2B in BAT Activation and Aging

(A and B) Interscapular surface temperature quantified by infrared thermography (A) and relative oxygen consumption at 4°C (B) of ATA2B-KO and Con-A2B mice (n = 5).

(C and D) PET/MRI [^{18}F]FDG uptake imaging (C) and quantification (D) of mice treated with vehicle, NE (1 mg/kg), or A2B agonist (0.1 mg/kg) (n = 4). Arrows indicate interscapular BAT.

(E) Expression of aging markers in BAT of ATA2B-KO and Con-A2B mice (n = 6).

(F and G) Abundance of malondialdehyde (F) and senescence-associated beta-galactosidase activity (G) in BAT of ATA2B-KO and Con-A2B mice (n = 6).

(H) Expression of oxidative metabolism and BAT whitening marker genes of ATA2B-KO and Con-A2B mice (n = 6).

(I) Representative H&E stain of BAT of aged ATA2B-KO and Con-A2B mice (scale bar, 100 μm).

(J and K) Time course (J) and average (K) of whole-body O_2 consumption of ATA2B-KO and Con-A2B mice at 23°C (n = 5).

*$p < 0.05$. Data are shown as mean + SEM (J) or boxplot (with median) and whiskers (1.5× interquartile range) (A, B, D–H, and K) and were analyzed with two-tailed Student's t test (A, B, E–H, and K) or ANOVA with Newman-Keuls post hoc test (D).

See also Figure S2.

malondialdehyde (MDA), a marker of oxidative stress and lipid peroxidation, were more abundant in A2B-deficient BAT (Figure 2F). Furthermore, activity of SA-BetaGal was significantly increased in BAT from ATA2B-KO mice (Figure 2G), showing that loss of A2B enhances senescence of BAT.

Importantly, BAT from ATA2B-KO showed decreased expression of VEGF-A, a major proangiogenic cytokine, as well as reduced expression of genes important for mitochondrial function and oxidative metabolism (Figure 2H), a pattern reminiscent of BAT changing its phenotype toward white fat, a process also termed "whitening" (Shimizu et al., 2014). In line with these expression data, histological analysis of BAT from aged ATA2B-KO mice revealed enlarged fat droplets compared to BAT from Con-A2B (Figure 2I), indicating enhanced BAT whitening in the absence of A2B.

To study whether pharmacological activation of A2B might counteract aging processes in BAT, we treated 20-month-old wild-type mice with the A2B agonist. A2B stimulation had significant beneficial effects on the expression of markers for aging and senescence, restoring expression to levels similar to those observed in young animals (Figures S2J and S2K). Notably, levels of MDA (Figure S2L) and SA-BetaGal activity (Figure S2M) were significantly decreased in BAT from wild-type mice treated with A2B agonist, indicating reduced oxidative stress, lipid peroxidation, and tissue senescence. Overall, these changes in marker genes were accompanied by changes in BAT function: whole-body oxygen consumption of aged ATA2B-KO mice was significantly reduced compared to aged Con-A2B animals (Figures 2J and 2K), while locomotor activity was unaffected (Figure S2N).

In summary, these data indicate that loss of A2B aggravates—while A2B stimulation alleviates—aging-related processes and whitening in murine BAT.

Molecular Mechanisms: A2B Heterodimerization and Its Role in Adenosine Signaling

The finding that A2B activates BAT was unexpected given our previous finding that A2A stimulation results in BAT activation (Gnad et al., 2014). Therefore, we studied the mechanisms of A2B signaling. In light of the short half-life of adenosine *in vivo*, we so far used A2B-specific small molecule agonists. To study the physiological significance and molecular mechanisms of A2B signaling for adenosine-induced effects, we used our established murine *in vitro* brown adipocyte (BA) model (Haas et al., 2009). To further delineate the role of A2B and A2A for adenosine signaling in BAs, we first simultaneously blocked A2B and A2A, which fully abrogated adenosine-mediated lipolysis (Figure S3A). Next, we analyzed lipolysis after pharmacological blocking of the individual receptors: as expected (Gnad et al., 2014), we found strongly decreased sensitivity to adenosine in BAs treated with an antagonist specific for A2A (Figure S3B).

Surprisingly, adenosine-mediated BA activation was suppressed when cells were pre-treated with an antagonist specific for A2B (Figure 3A). Moreover, adenosine-induced oxygen consumption was lost in BAT isolated from ATA2B-KO mice (Figure 3B), as well as after acute pharmacological blockade of A2B (Figure S3C). Similar data were obtained with BAs deficient for A2B (Figure S3D) or A2A (Figure S3E). Together, these data show that both adenosine receptors mediate adenosine effects in murine BAs and that A2B has a permissive effect on A2A-mediated adenosine signaling. This complete dependence of adenosine-induced effects on A2B was unexpected since adenosine can enhance murine and human BAT activity via the adenosine A2A receptor (Gnad et al., 2014; Lahesmaa et al., 2019; Ruan et al., 2018).

Regarding the molecular mechanism and the interaction between A2B and A2A, a previous report indicated that overexpressed A2B inhibits signaling of A2A (Hinz et al., 2018); thus, ablation of A2B should increase rather than suppress adenosine effects. Interestingly, the stimulatory effect of an A2A-specific agonist (CGS21680; 1 mg/kg) on EE was fully blunted in ATA2B-KO mice (Figures 3C and S3F) as well as after pharmacological blockade of A2B *in vivo* (Figures S3G and S3H). Therefore, we analyzed the molecular interaction between A2B and A2A in more detail to scrutinize the permissive role of A2B in adenosine signaling. Bioluminescence resonance energy transfer (BRET) analysis showed specific molecular A2B/A2A interaction in both murine and human BA as well as in C2C12 myocytes (Figures 3D, S3I, and S3J). *In situ* proximity ligation assay revealed co-localization of endogenous A2B and A2A receptors in BAT (Figure 3E). Molecular modeling indicated that transmembrane (TM) regions 5 and 6 of both receptors could be critical for heterodimerization (Figures 3F, S3K, and S3L). To test the role of TM5 and 6 for heterodimerization directly, peptides derived from TM regions 5 and 6 of both receptors were applied, which abrogated adenosine-induced BA activation (Figure 3G), demonstrating the functional relevance of these regions/interactions. Moreover, site-directed mutagenesis of amino acid residues predicted *in silico* (Figure 3H) blunted A2B/A2A BRET signals (Figure 3I). No differences in A2B-activated lipolysis between control and A2A-deficient BA and BAT explants were detected, indicating that A2B can activate EE independently of A2A (Figures S3M and S3N).

A2B Stimulation Counteracts Diet-Induced Obesity

Given the importance of A2B for EE in both SKM and BAT of lean mice, we asked whether the A2B stimulation could be used to treat DIO. A2B is expressed abundantly in both murine SKM and BAT of obese mice (Figures S4A and S4B), indicating that A2B could be targeted to increase EE also in obesity. Diet-induced weight gain was significantly reduced by A2B stimulation (Figure 4A) accompanied by improved glucose tolerance (Figures 4B and S4C), while food intake was similar (Figure S4D). Importantly, A2B stimulation had no adverse effects on heart rate (Figure 4C) and blood pressure (Figures S4E and S4F), which is in stark contrast to previous studies focusing on beta-AR stimulation (Cypess et al., 2015). Moreover, analysis of clinical chemistry parameters showed no significant differences between vehicle and A2B agonist-treated mice (Table S5).

A2B agonist-treated DIO mice exhibited a significant increase in muscle and lean mass (Figures 4D, S4G, and S4H). Additionally, the major physiological readout for muscle function—muscle force—as measured *in vivo* and *ex vivo* was significantly increased in A2B agonist-treated obese mice (Figures 4E and 4F). These functional effects were mirrored by significantly increased expression of MyHCI, IIa, and IIb (Figure S4I), as well as of MyoD, Mef2c, and alpha1-actin (Figure S4J). Parallel to the increase in muscle mass, white adipose tissue (WAT) mass was reduced in A2B agonist-treated mice on high-fat diet (HFD) (Figures 4G and S4K). Although BAT mass was not affected (Figure S4L), BAT exhibited increased thermogenic (Figure 4H) and mitochondrial marker gene (Figure 4I) expression. Moreover, whitening of BAT was reduced in A2B-treated mice on HFD (Figure 4J). Notably, A2B agonist treatment induced browning of WAT as indicated by increased expression of UCP-1—the master thermogenic protein specifically expressed in brown/beige adipocytes (Figures 4K, 4L, and S4M). This browning effect was cell autonomous, since thermogenic genes were significantly upregulated in primary white adipocytes after A2B stimulation (Figure S4N). Recently, mast cell inactivation has been described to promote browning of WAT in mice (Zhang et al., 2019). Furthermore, A2B signaling has been linked to mast cell activation. However, conflicting data have been published (Hua et al., 2013; Ryzhov et al., 2008). Mast cell activation after pharmacological stimulation with Bay 60-6583 had no effect on mast cell degranulation (Figure S4O). Moreover, C48/80-induced mast cell degranulation was unaffected by A2B agonist treatment (Figure S4O), further underlining the cell-autonomous effect of A2B on beige fat. Overall, A2B treatment strongly increased whole-body EE in mice on HFD by 49% (Figure 4M), while locomotor activity was not affected (Figure S4P).

Taken together, pharmacological A2B stimulation counteracts HFD-induced obesity by positively affecting whole-body EE. Moreover, A2B treatment results in increased mass and force of SKM, thermogenic capacity of BAT, and browning of WAT.

A2B in Human BAT and SKM

Finally, the role of A2B was studied in human BAT and SKM. Human BAT biopsies exhibited high A2B expression in lean

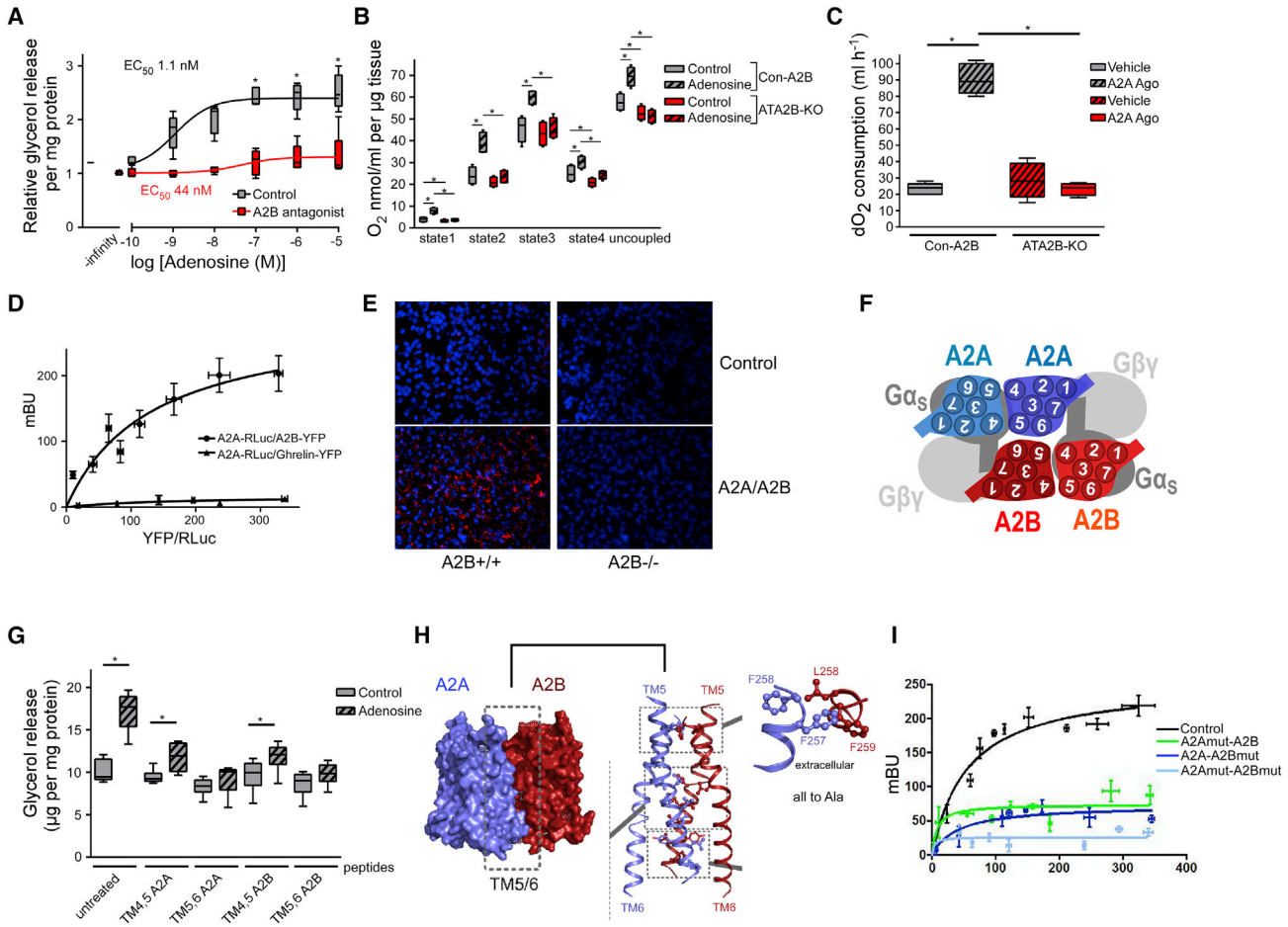

Figure 3. A2B Heterodimerization

(A) Lipolysis of murine BA treated with adenosine in the presence or absence of A2B antagonist (PSB603; 150 nM) (n = 6).

(B) O_2 consumption of BAT explants deficient for A2B and treated with adenosine (1 µM) (n = 6).

(C) O_2 consumption of ATA2B-KO and Con-A2B mice injected with vehicle or A2A agonist (CGS21680; 1 mg/kg) (n = 5).

(D) BRET analysis of A2A-RLuc and A2B-YFP or A2A-RLuc and Ghrelin-YFP in murine BAs (n = 4).

(E) Representative image after A2B/A2A proximity ligation assay in murine BAT.

(F) *In silico* model of A2B/A2A quaternary structure.

(G) Lipolysis of murine BA treated with adenosine (1 µM) in the presence of indicated TM peptides (100 µM) (n = 4).

(H) *In silico* model of amino acid residues involved in A2B/A2A heterodimerization.

(I) A2B/A2A BRET after site-directed mutagenesis of residues identified in (H) (n = 4).

*$p < 0.05$. Data are shown as boxplot (with median) and whiskers (1.5× interquartile range) (A–C and G) or mean + SD (D and I) and analyzed using two-tailed Student's t test (A) or ANOVA with Newman-Keuls post hoc test (B, C, and G).

See also Figure S3.

subjects, while A2B expression was significantly less abundant in BAT from overweight individuals (Figure 5A; Table S6). Interestingly, A2B expression in human BAT significantly inversely correlated with age (Figure 5B), as well as with total body fat mass (Figure 5C), and positively correlated with UCP-1 expression (Figure 5D). Human BAT activity was directly measured in the same cohort of human subjects using [^{18}F]FDG imaging. Human subjects with low detectable BAT activity (low BAT; Figures 5E and 5F) had lower levels of A2B expression in BAT than subjects with high BAT activity (high BAT; Figures 5E and 5F). A2B expression significantly correlated with glucose uptake in high BAT subjects (Figure 5G). On a cellular level, primary human BA lipolysis was significantly activated by A2B stimulation (Figure S5A) and by adenosine in an A2B-dependent manner (Figure S5B). To further study whether A2B expression differs between human BAT and WAT, subcutaneous WAT biopsies from a cohort of 405 individuals were analyzed. Similar to human BAT, a significant inverse correlation of A2B expression with BMI was found (Figure S5C). Further histological analysis of WAT from 10 individuals of this cohort with the highest and lowest A2B expression (Table S7) revealed significantly decreased human adipocyte cell diameter—a measure for lipid load and hypertrophy—when A2B expression was high (Figures 5H and S5D). Expression of UCP-1 and other marker genes selective for human thermogenic and beige cells Tbx1, Cidea, and P2rx5 (Jespersen et al., 2013; Ussar et al., 2014) positively

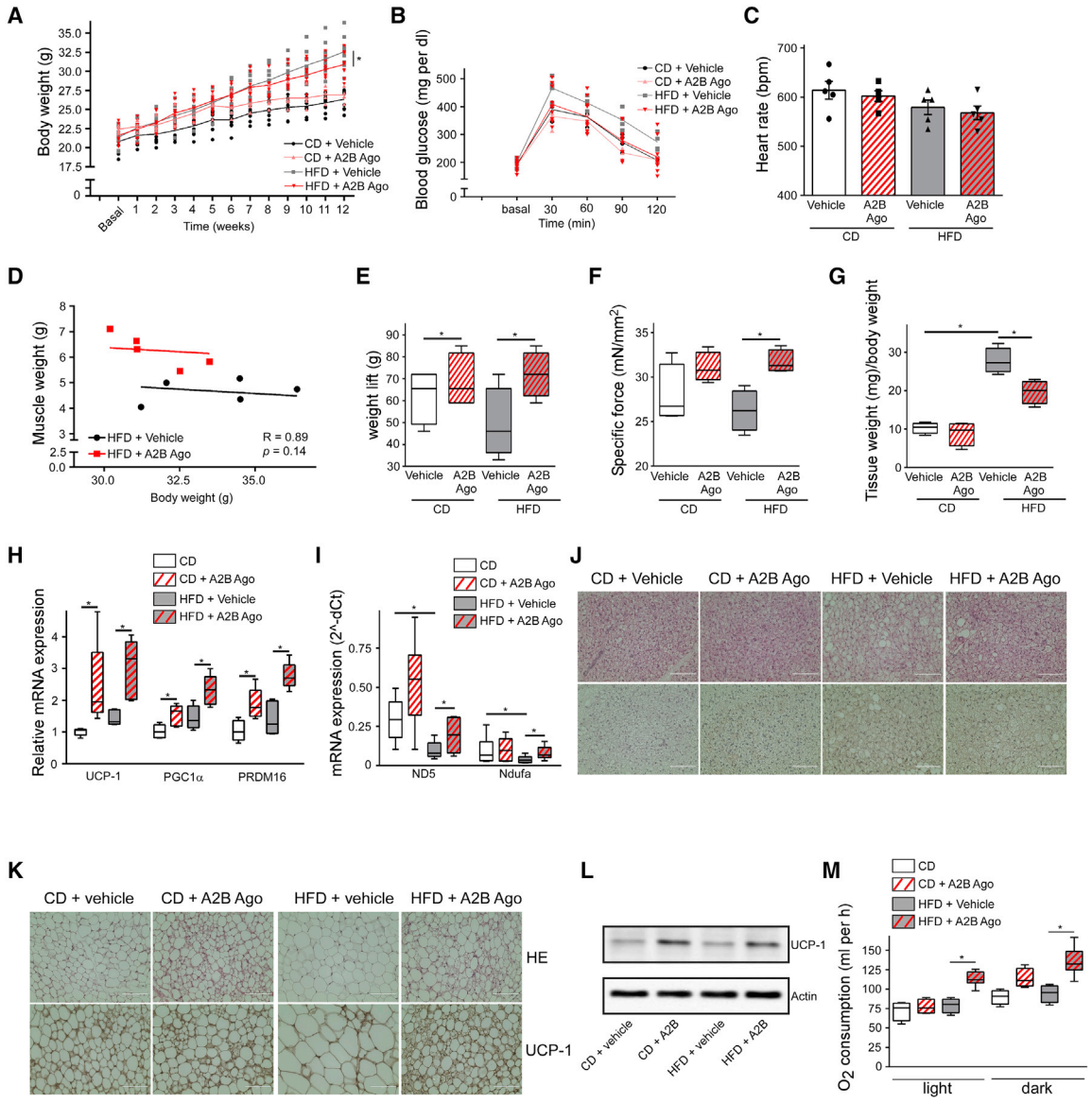

Figure 4. A2B Treatment Counteracts DIO

Twelve-week DIO study with A2B stimulation: body weight (A), glucose tolerance (B), heart rate (C), correlation of muscle mass/body weight (D), weight lift (E), *ex vivo* specific muscle force (F), inguinal WAT mass (G), thermogenic (H) and mitochondrial (I) marker gene expression in BAT, representative H&E (top) or UCP-1 (bottom) stain of BAT (J) and inguinal WAT sections (K) (scale bar, 100 μm), UCP-1 immunoblot of inguinal WAT (L), and O_2 consumption at 23°C (M). n = 5 per group. *p < 0.05. Data are shown as mean + SEM (A–C), scatterplot (D), or boxplot (with median) and whiskers (1.5× interquartile range) (E–I and M) and analyzed using ANCOVA (D) or ANOVA with Newman-Keuls post hoc test (A, C, E–I, and M).
See also Figure S4.

correlated with A2B expression in human WAT (Figures 5I and S5E–S5G). In summary, these data indicate that A2B expression correlates with EE of human BAT as well as with human WAT browning and that individuals with low A2B levels might be more prone to obesity.

To study A2B function in aging of human SKM, we first studied A2B expression in muscle biopsies from overweight or obese type 2 diabetic subjects (cohort 1) and found declining A2B expression with age (Figure 5J; Table S8). Similar results were obtained in SKM biopsies from highly competitive former master athletes (cohort 2; Figure S5H; Table S9). In contrast to A2B, no correlation between age and expression of the G_s-coupled beta2- or beta3-AR, which have inotropic effects (references in Cairns and Borrani, 2015), could be detected (Figure S5I). Importantly, A2B expression positively correlated with basal oxygen consumption in human SKM explants (Figure 5K), whereas no significant correlation between EE and expression was found for beta2- or beta3-AR, respectively (Figures S5J and S5K). Further analyses revealed that A2B expression positively correlated with marker genes of oxidative metabolism (Figures 5L and S5L) and satellite marker Pax7 (Figure S5M), whereas A2B abundance negatively correlated with expression of senescence

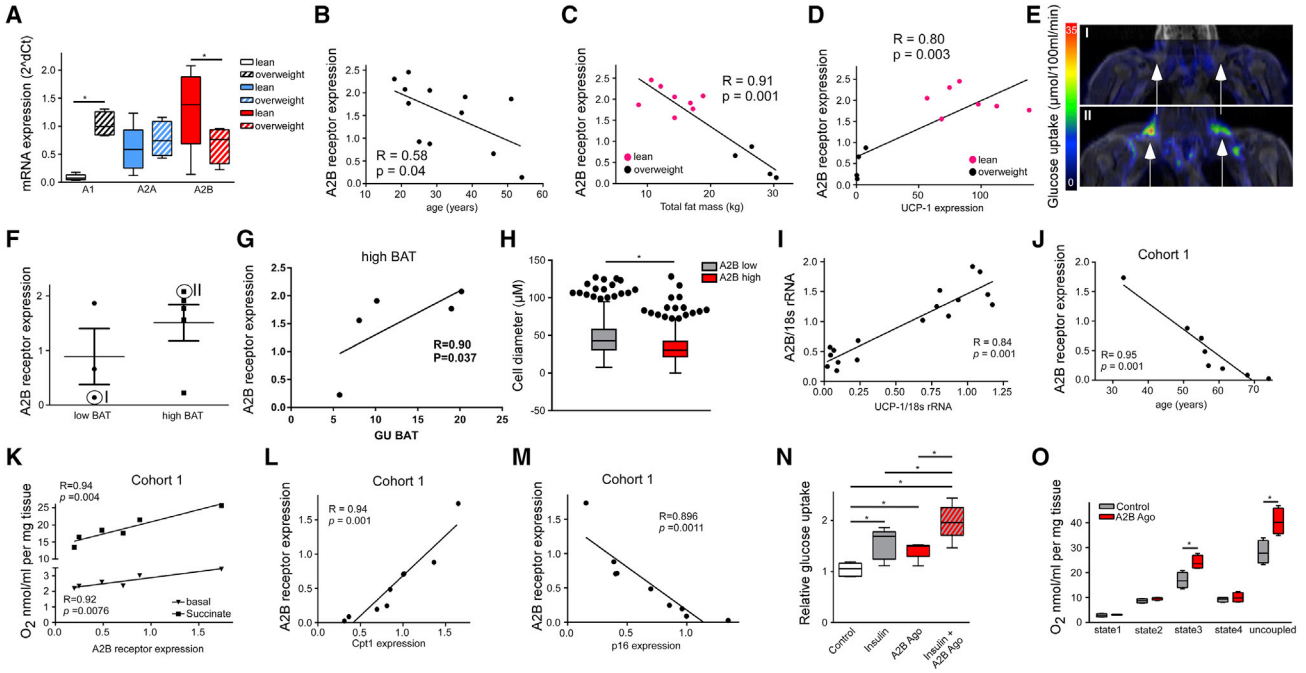

Figure 5. A2B Signaling in Human BAT and SKM

(A) Adenosine receptor expression in human BAT of lean (n = 8) and overweight subjects (n = 4).

(B–D) BAT A2B expression correlated with age (B), total body fat mass (C) (n = 12), or UCP-1 expression (D) (n = 11).

(E) Representative PET/ MRI image of [^{18}F]FDG uptake of one low BAT and high BAT subject from (D).

(F) A2B expression in low BAT and high BAT subjects.

(G) Correlation of [^{18}F]FDG uptake with A2B expression of high BAT subjects (n = 5).

(H and I) Mean adipocyte diameter (n = 405) (H) and A2B/UCP-1 correlation (I) from 10 subjects with high or low A2B expression, respectively, in subcutaneous WAT.

(J) Correlation of A2B expression with age in human SKM (n = 9).

(K) Basal and succinate-fueled O_2 consumption in human SKM correlated with A2B expression (n = 6).

(L and M) Correlation of A2B expression with oxidative marker Cpt1 (L) or senescence marker p16 (M) in SKM (n = 9).

(N) Glucose uptake of primary human myocytes treated with A2B agonist (300 nM), insulin (100 nM), or both (n = 5).

(O) O_2 consumption of human SKM explants treated with A2B agonist (300 nM) (n = 3).

*$p < 0.05$. Data are shown as mean + SEM (F), scatterplot (B–D, G, and I–M), or boxplot (with median) and whiskers (1.5× interquartile range) (A, H, N, and O). (H) also shows outliers. Data were analyzed with ANOVA with Newman-Keuls post hoc test (A and N), Pearson correlation coefficient (B–D, G, and I–M), or two-tailed Student's t test (H and O).

See also Figure S5.

markers p16 and p21 (Figures 5M and S5N). On a cellular level, A2B activation significantly enhanced expression of markers for oxidative metabolism (Figure S5O) and myocyte differentiation (Figure S5P), as well as of satellite marker genes (Figure S5Q) in primary human myocytes. Moreover, MyHCI, MyHCIIa, and IIb isoform expression was significantly upregulated after stimulation with an A2B agonist (Figure S5R). These data show that A2B expression inversely correlates with aging-related processes and senescence in human SKM.

Functionally, pharmacological A2B stimulation significantly elevated basal and insulin-stimulated glucose uptake of primary human myocytes (Figure 5N). Moreover, adenosine and A2B stimulation significantly increased glycolysis, reaching up to 66% and 78% of the maximal glycolytic rate, respectively (Figure S5S). Also, stimulation of A2B significantly enhanced EE in human myocytes (Figure S5T). Importantly, treatment of human SKM biopsies with A2B agonist resulted in significantly increased EE (Figure 5O). Thus, A2B activation enhances human muscle quality including fiber composition, oxidative metabolism, glucose uptake and utilization, and EE.

DISCUSSION

SKM and adipose tissue are closely linked via multiple signaling pathways, and inter-organ communication is an evolving concept for regulation of both tissues and whole-body energy homeostasis (Boström et al., 2012; Dong et al., 2016; Kalinkovich and Livshits, 2017; Kong et al., 2018; Trayhurn et al., 2011). The main physiological function of BAT is non-shivering thermogenesis as a response against cold in newborn and infants. Moreover, active BAT is also present in human adults. Adipocytes with brown-like features have also been found in human WAT and these (so-called beige or brite) adipocytes (Kajimura et al., 2015; Pfeifer and Hoffmann, 2015) contribute to whole-body metabolism (Wu et al., 2012).

BAT also has endocrine functions and secretes adipokines—so-called batokines (Villarroya et al., 2017)—that can affect

SKM insulin signaling (Nicholson et al., 2018). The batokine FGF-21 is of particular interest, since it has been shown to increase glucose uptake in murine SKM and human myocytes (Mashili et al., 2011). In addition, inflamed adipose tissue releases pro-inflammatory cytokines that play a major role in SKM insulin resistance (Zamboni et al., 2008). There is also evidence that the crosstalk between BAT and muscle regulates exercise capacity and BAT-dependent EE: inactivation of BAT by housing mice in thermoneutrality induces expression of myostatin—a known inhibitor of myogenesis and SKM function—in BAT, thereby reducing exercise capacity (Kong et al., 2018). Vice versa, several exercise-regulated myokines like irisin, meteorin-like, or β-aminoisobutyric acid are potent inducers of WAT browning in rodents (Pedersen and Febbraio, 2012; Stanford and Goodyear, 2016). Nevertheless, the effect of exercise on browning of human WAT is still debated (Stanford and Goodyear, 2016).

Our studies indicate that adenosine might also be involved in the crosstalk between muscle and BAT. Adenosine is released by both BAT activation and SKM contraction (Gnad et al., 2014; Hellsten et al., 1998) and might serve as an autocrine enhancer of both processes in a positive feedforward manner. SKM is in close vicinity to supraclavicular BAT and subcutaneous WAT, which is the major site of beige/brite adipocytes (Rosenwald and Wolfrum, 2014).

Adenosine signaling in muscle is linked to the sympathetic nervous system (SNS). The SNS enhances SKM contraction and has pro-hypertrophic effects (Berdeaux and Stewart, 2012; Roatta and Farina, 2010) via norepinephrine-mediated beta2-AR activation (references in Berdeaux and Stewart, 2012). However, long-term administration of beta2-AR agonists has detrimental effects on the heart (Moore et al., 1994), thereby hindering its use against sarcopenia. Apart from norepinephrine, neurons of the SNS release other transmitters including ATP. ATP is quickly metabolized to adenosine, which itself signals through four receptor subtypes: A1, A2A, A2B, and A3 (Fredholm et al., 2001, 2011; Ralevic and Burnstock, 1998). These receptors are coupled to either G_i (A1 and A3) or G_s (A2A and A2B) proteins that inhibit or activate cAMP production, respectively (Fredholm et al., 2001). In human SKM tissue, A2A and A2B receptors are highly expressed (Lynge and Hellsten, 2000). Our data show that A2B is the most highly expressed adenosine receptor in human and murine SKM cells and that A2B mediates the largest part of the adenosine-induced increase in cAMP. *In vivo*, both young and old SKM-specific A2B knockout mice exhibited a significant decrease in muscle mass. Conversely, treatment of mice with a specific A2B agonist significantly increased muscle mass in young and aged wild-type mice. Importantly, A2B stimulation for 4 weeks in aged mice brought muscle mass back to levels observed in young mice.

One of the most remarkable features of SKM is its plasticity and its capacity to regenerate (Dumont et al., 2015), which strongly depends on muscle satellite cells (Dumont et al., 2015). Treatment of mice with the A2B agonist significantly increased the number of muscle satellite cells. Age-related changes in muscle are not confined to a mere decline in muscle mass but also include a decline in muscle quality and function (Barbat-Artigas et al., 2012). In addition, decline in strength rather than muscle quantity is associated with the development of disability and overall mortality (Newman et al., 2006). It is of special interest in this context that treatment with the A2B agonist restored muscle force in aged mice to levels of young mice. Thus, our data indicate that A2B plays an unexpected protective role in aging muscle. The role of beta-AR signaling during aging SKM is debated. Some studies report no age-related alteration in beta-AR signaling (Elfellah et al., 1989; Kendall et al., 1982), whereas other studies suggest an age-dependent loss of beta-AR responsiveness (Ford et al., 1992, 1995). In our hands, beta2- and beta3-AR abundance in human SKM did not correlate with age. Functionally, basal EE from muscle did not correlate with beta-AR expression. In contrast, those subjects with high A2B expression exhibited high basal SKM-dependent EE, indicating that high A2B expression in human SKM might protect from age-related decline of SKM function. Aerobic capacity and mitochondrial function decline with aging in humans (Fleg et al., 2005; Short et al., 2005), especially in tissues with high energy demand (Boengler et al., 2017) like SKM and BAT. A2B activation significantly elevated genes involved in mitochondrial biogenesis and function, as well as in oxidative metabolism in murine SKM and in primary human myocytes. SKM takes up a large proportion of glucose (Richter and Hargreaves, 2013) and therefore loss of muscle mass is a risk factor for insulin resistance (Bijlsma et al., 2013; McGregor et al., 2014). Stimulation of A2B induced glucose uptake in primary human muscle cells comparable to insulin and had an additive effect on insulin-mediated glucose uptake.

Overall, our studies show that the A2B signaling pathway has a major positive effect on muscle and counteracts age-related decline in SKM mass and function. In parallel, A2B signaling enhances EE in murine and human myocytes and SKM biopsies.

Regarding the role of adenosine in BAT, it is well established that adenosine is a major regulator of cAMP signaling and lipolysis in adipose tissues. During SNS activation, adenosine is released in BAT. Moreover, BAs in cell culture release adenosine after activation of cAMP signaling (Gnad et al., 2014). In WAT, adenosine signals mainly via the G_i-coupled A1 receptor and, therefore, adenosine reduces cAMP levels and lipolysis (Gnad et al., 2014; Johansson et al., 2008). In BAT, the picture is more complicated since there are important species differences: adenosine inhibits BAT activation in hamster whereas it activates lipolysis and EE in human and murine BAT (Gnad et al., 2014).

Although much of our knowledge of BAT is based on mouse studies, there is an ongoing debate about differences between murine and human BAT, especially regarding the "identity" of BAT in human adults in relation to murine classical BAT and beige fat. The composition of human BAT and the type of adipocytes present in thermogenic fat depots appear to depend on age (Kajimura et al., 2015): adipocytes found in interscapular BAT of human infants express markers that are characteristic of classical BAs (Lidell et al., 2013). In contrast, BAT depots of adult humans are generally more heterogeneous, containing UCP1-positive and -negative adipocytes (Cypess et al., 2013; Virtanen et al., 2009). Moreover, the anatomic localization plays an important role: BAs have been detected in autopsy studies to be more concentrated around deeper organs of the body, consistent with the function of a "thermogenic jacket" (Heaton, 1972). Adult supraclavicular BAT appears to more closely resemble murine beige adipocytes (Shinoda et al., 2015; Wu et al., 2012), while other BAT depots—including cervical and

perirenal regions—consist of adipocytes that express classical brown markers like ZIC1 (Cypess et al., 2013; Kajimura et al., 2015).

So far, not much was known about the physiological function of the A2B receptor in BAT. Adipose tissue-specific ablation of A2B resulted in an abrogation of BAT function with reduced body temperature in newborn mice, as well as a decrease in whole-body O_2 consumption by approximately 30%. Conversely, treatment with the A2B agonist increased murine BAT activity and O_2 consumption. Given the protective role of A2B signaling in age-related decline of SKM, we also studied its role in BAT during aging. BAT function and BAT mass decline with aging and obesity (Enerbäck, 2010; Kajimura et al., 2015), and BAT takes on the appearance of white fat, a process known as "whitening." Overall, A2B-deficient BAT exhibited a phenotype that can be summarized as advanced aging and increased "whitening," which was reflected in reduced EE.

Given our findings of A2B-mediated increase of EE in SKM and BAT, we studied whether A2B might also be relevant in obesity. Impressively, the A2B agonist increased whole-body oxygen consumption by 49%, resulting in a significant reduction of WAT mass and improved glucose metabolism. Moreover, A2B agonist-treated animals on HFD exhibited a significant increase in SKM mass and strength. In parallel, A2B agonist treatment improved DIO-induced whitening of BAT and enhanced browning of WAT. Moreover, A2B agonist treatment induced thermogenic genes in primary murine white adipocytes, showing a cell-autonomous effect of A2B on browning. Recently, a role of mast cells has been described in browning of murine WAT and mast cell inactivation promotes browning of subcutaneous WAT concomitant with increased energy expenditure (Zhang et al., 2019). Conflicting reports have been published about the role of A2B on mast cell activation: analysis of mast cells from A2B-deficient mice revealed a pro-inflammatory role of A2B (Ryzhov et al., 2008). In contrast, a study using a combination of pharmacological stimulation with the unspecific adenosine receptor agonist NECA and genetic models showed that A2B reduces mast cell degranulation (Hua et al., 2013). Using the specific A2B agonist Bay 60-6583, we found no effect of A2B stimulation on mast cell degranulation. Apart from the direct effect of A2B on EE in brown/beige fat and SKM, A2B should have further additive positive effects on obesity-induced inflammation by promoting alternative macrophage maintenance (Csóka et al., 2014) and insulin signaling (Johnston-Cox et al., 2012).

In human BAT, we found that A2B expression positively correlates with UCP-1 abundance and high BAT activity. In contrast, A2B abundance negatively correlates with aging. Interestingly, A2B was significantly downregulated in overweight subjects, whereas the inhibitory A1 receptor was significantly upregulated. Together, this altered ratio of inhibitory A1 and stimulatory A2B might be unfavorable for BAT-mediated EE in human obesity.

Of note, A2B stimulation had no adverse effects on heart rate and blood pressure in contrast to previous studies using beta-AR stimulation to enhance EE (Cypess et al., 2015). Analysis of a broad range of clinical chemistry parameters revealed no significant changes between vehicle and A2B agonist-treated mice, indicating no adverse effects. Together these data indicate that the adenosine/A2B pathway might be an important alternative to beta-adrenergic drugs. Regarding the selectivity of the A2B agonist used in this study: Bay 60-6583 is the most specific A2B agonist (EC_{50} 2.83 nM; Baraldi et al., 2008) currently available and frequently used in *in vitro* and *in vivo* studies. Although previous competition binding assays (Alnouri et al., 2015) for rodent A1 and A2B heterologously overexpressed in CHO cells indicate binding of Bay 60-6583 to the A1 receptor at very high concentrations, further studies (Eckle et al., 2007) on the functional relevance of a potential cross-activation of A1 by Bay 60-6583 clearly showed no significant effect even at concentrations far beyond the 300 nM used in our study. Nevertheless, to address the physiological relevance of a potential interaction of Bay 60-6583 with A1 receptor in BAs, we performed dose-response analysis using lipolysis as functional readout. Importantly, no shift in dose response was observed following A2B stimulation after short hairpin RNA (shRNA)-mediated A1 knockdown (EC_{50} 2.64 nM versus 2.74 nM; Figure S5U). Together, these data show that there is no significant contribution of A1 at the Bay 60-6583 concentrations used in our experiments.

Given the dominant role of A2B in adenosine signaling, we further scrutinized its interaction with other adenosine receptors. AdoR homo- and heterodimers have been described (Canals et al., 2004; Carriba et al., 2007; Ciruela et al., 1995, 2001; Ginés et al., 2000). Heterodimers between G_s-coupled GPCRs are scarce and have so far been reported only after overexpression (Breit et al., 2004; Fuenzalida et al., 2014; Lavoie et al., 2002). An interaction between A2A and A2B was previously postulated because overexpression of A2A in HEK cells improved cell surface expression of A2B (Moriyama and Sitkovsky, 2010). However, we did not observe a reduction in A2B protein levels of A2A-deficient BAT membranes (Figure S3O). Although a recent report showed that A2B negatively modulates A2A pharmacology in overexpressing HeLa and Jurkat cells (Hinz et al., 2018), we found in primary adipocytes and SKM cells that A2B is necessary for adenosine/A2A signaling. Importantly, we identify the major domains and amino acid residues within transmembrane regions 5 and 6 of the receptors that are required for heterodimerization. On a molecular level, A2B might be important for the conformation of the adenosine/A2A agonist binding site of A2A. Moreover, A2B might be necessary for the assembly of the cAMP-signalosome downstream of A2A.

Taken together, our data demonstrate that the adenosine/A2B signaling pathway plays a central role in maintaining SKM mass and function. Stimulation of A2B counteracted age-related and obesity-associated sarcopenia and restored SKM function and mass to juvenile levels. In parallel, A2B activation was also relieving age- and obesity-related decline in BAT function and induced browning of WAT. Together, our data indicate that targeting this single receptor might be a novel, holistic approach toward healthy aging and metabolic balance.

Limitations of Study

The A2B receptor is not only expressed in SKM and BAT but also in several other organs including brain, liver, and lung, albeit at lower levels. Thus, the effects of the A2B agonist observed *in vivo* might not be confined to SKM and BAT. Although we observed no adverse effects after prolonged pharmacological A2B stimulation in mice, the widespread expression of A2B might be a problem concerning potential side effects of A2B agonists in humans. Although the A2B agonist used had no effect in A2B null adipocytes and in BAT and SKM of global knockout mice, not

all agonist studies were performed in tissue-specific knockouts. The fact that we observed significant differences in the expression of adenosine receptors in BAT of overweight human subjects, but not in obese mice, indicates that there could be species differences. While our data point to a positive role of adenosine/A2B in aging of muscle and BAT, future work is required to study its role in longevity.

STAR★METHODS

Detailed methods are provided in the online version of this paper and include the following:

- KEY RESOURCES TABLE
- RESOURCE AVAILABILITY
  - Lead Contact
  - Materials Availability
  - Data and Code Availability
- EXPERIMENTAL MODEL AND SUBJECT DETAILS
  - Mice
  - Human Studies
  - Cells
- METHOD DETAILS
  - BAT [^{18}F]FDG-PET imaging
  - Human BAT Biopsy Procedures
  - Skeletal Muscle Isolation and Force Measurement
  - *In Vivo* Weight Lift
  - Forelimb Grip Test
  - Measurement of Endogenous Respiration
  - Glucose Uptake Assay
  - Beta-Hexosaminidase Release/Degranulation Assay
  - Glycolysis
  - Senescence-Associated Beta-Galactosidase Activity Assay
  - Lipolysis Assay
  - Immunoblot
  - RNA Isolation and qPCR
  - Bioluminescence Resonance Energy Transfer
  - Peptide Design
  - Pharmacological Activation of Energy Expenditure
  - Physiological Activation of Energy Expenditure
  - PET/MRI of BAT Activation
  - Body Composition Analysis
  - Glucose Tolerance Test
  - Thermography
  - Satellite Cell Isolation
  - Immunohistochemistry and PLA
  - Molecular Modeling
  - Site-Directed Mutagenesis
- QUANTIFICATION AND STATISTICAL ANALYSIS

SUPPLEMENTAL INFORMATION

Supplemental Information can be found online at https://doi.org/10.1016/j.cmet.2020.06.006.

ACKNOWLEDGMENTS

We thank Elena Weidner, Angelika Wassmuth, Daniela Hass, Patricia Zehner, Mojgan Ghilav, Bianca Collins, and Frank Holst for technical assistance. This work was funded by the Deutsche Forschungsgemeinschaft (DFG, German Research Foundation) project number 289107305 to T.G.; 214362475/GRK1873/2 to L.R.-S., S.H.-B., F.C., and A.P.; and 335447717/SFB1328, project A09 to A.P. The human BAT study was supported by Academy of Finland, the Paulo Foundation, the Finnish Cultural Foundation Southwest Finland Regional Fund, the Turku University Hospital Research Funds, and the European Union. The Centre for Physical Activity Research (CFAS) is supported by TrygFonden (grants ID 101390 and ID 20045) Novo Nordisk Foundation Center for Basic Metabolic Research is an independent Research Center, based at the University of Copenhagen, Denmark, and partially funded by an unconditional donation from the Novo Nordisk Foundation (https://cbmr.ku.dk/) (grant number NNF18CC0034900). N.Z.J. was supported by the Danish Diabetes Academy/Novo Nordisk Foundation. H.K.E. was supported by the National Institutes of Health grants R01DK122796, R01DK109574, and R01HL133900. J.R. is also affiliated with the Department of Pediatrics and Adolescent Medicine, University of Cologne, Cologne, Germany; B.K.F. and A.P. are members of the PharmaCenter Bonn, University of Bonn, Germany.

AUTHOR CONTRIBUTIONS

Conceptualization, T.G. and A.P.; Methodology, G.N., A.C., L.P., and R.F.; Formal Analysis, T.G., M.L., G.N., L.R.-S., M.K., W.D.-C., P.B., M.B., and K.A.V.; Investigation, T.G., G.N., M.L., L.R.-S., F.C., A.C., J.N., A.H., S.H.-B., F.S., M.T., V.T., C.B., M.K., W.D.-C., P.B., M.B., and L.P.; Resources, G.N., N.Z.J., C.S., C.B., J.R., C.D., T.N., M.T., M.B., L.P., D.W., P.N., H.K.E., B.K.F., R.F., W.B., K.A.V., and A.P.; Writing – Original Draft, T.G. and A.P.; Writing – Review & Editing, T.G., P.N., L.P., B.K.F., R.F., L.R.-S., M.F., C.B., W.B., K.A.V., and A.P.; Visualization, T.G., A.C., L.P., and A.P.; Supervision, T.G. and A.P.; Project Administration, A.P.; Funding Acquisition, T.G., P.N., K.A.V., and A.P.

DECLARATION OF INTERESTS

T.G., L.R.-S., F.C., D.W., J.N., A.H., S.H.-B., B.K.F., and A.P. have filed an application for patenting A2B agonist treatment of musculoskeletal disorders.

Received: August 1, 2019
Revised: March 15, 2020
Accepted: June 8, 2020
Published: June 25, 2020

REFERENCES

Aherne, C.M., Saeedi, B., Collins, C.B., Masterson, J.C., McNamee, E.N., Perrenoud, L., Rapp, C.R., Curtis, V.F., Bayless, A., Fletcher, A., et al. (2015). Epithelial-specific A2B adenosine receptor signaling protects the colonic epithelial barrier during acute colitis. Mucosal Immunol. *8*, 1324–1338.

Alnouri, M.W., Jepards, S., Casari, A., Schiedel, A.C., Hinz, S., and Müller, C.E. (2015). Selectivity is species-dependent: characterization of standard agonists and antagonists at human, rat, and mouse adenosine receptors. Purinergic Signal. *11*, 389–407.

Baraldi, P.G., Tabrizi, M.A., Fruttarolo, F., Romagnoli, R., and Preti, D. (2008). Recent improvements in the development of A(2B) adenosine receptor agonists. Purinergic Signal. *4*, 287–303.

Barbat-Artigas, S., Rolland, Y., Zamboni, M., and Aubertin-Leheudre, M. (2012). How to assess functional status: a new muscle quality index. J. Nutr. Health Aging *16*, 67–77.

Barzilai, N., Huffman, D.M., Muzumdar, R.H., and Bartke, A. (2012). The critical role of metabolic pathways in aging. Diabetes *61*, 1315–1322.

Batsis, J.A., and Villareal, D.T. (2018). Sarcopenic obesity in older adults: aetiology, epidemiology and treatment strategies. Nat. Rev. Endocrinol. *14*, 513–537.

Berdeaux, R., and Stewart, R. (2012). cAMP signaling in skeletal muscle adaptation: hypertrophy, metabolism, and regeneration. Am. J. Physiol. Endocrinol. Metab. *303*, E1–E17.

Bijlsma, A.Y., Meskers, C.G., van Heemst, D., Westendorp, R.G., de Craen, A.J., and Maier, A.B. (2013). Diagnostic criteria for sarcopenia relate differently to insulin resistance. Age (Dordr.) *35*, 2367–2375.

Boengler, K., Kosiol, M., Mayr, M., Schulz, R., and Rohrbach, S. (2017). Mitochondria and ageing: role in heart, skeletal muscle and adipose tissue. J. Cachexia Sarcopenia Muscle *8*, 349–369.

Boström, P., Wu, J., Jedrychowski, M.P., Korde, A., Ye, L., Lo, J.C., Rasbach, K.A., Boström, E.A., Choi, J.H., Long, J.Z., et al. (2012). A PGC1-α-dependent myokine that drives brown-fat-like development of white fat and thermogenesis. Nature *481*, 463–468.

Breit, A., Lagacé, M., and Bouvier, M. (2004). Hetero-oligomerization between beta2- and beta3-adrenergic receptors generates a beta-adrenergic signaling unit with distinct functional properties. J. Biol. Chem. *279*, 28756–28765.

Brown, K., Xie, S., Qiu, X., Mohrin, M., Shin, J., Liu, Y., Zhang, D., Scadden, D.T., and Chen, D. (2013). SIRT3 reverses aging-associated degeneration. Cell Rep. *3*, 319–327.

Cairns, S.P., and Borrani, F. (2015). β-adrenergic modulation of skeletal muscle contraction: key role of excitation-contraction coupling. J. Physiol. *593*, 4713–4727.

Canals, M., Burgueño, J., Marcellino, D., Cabello, N., Canela, E.I., Mallol, J., Agnati, L., Ferré, S., Bouvier, M., Fuxe, K., et al. (2004). Homodimerization of adenosine A2A receptors: qualitative and quantitative assessment by fluorescence and bioluminescence energy transfer. J. Neurochem. *88*, 726–734.

Carriba, P., Ortiz, O., Patkar, K., Justinova, Z., Stroik, J., Themann, A., Müller, C., Woods, A.S., Hope, B.T., Ciruela, F., et al. (2007). Striatal adenosine A2A and cannabinoid CB1 receptors form functional heteromeric complexes that mediate the motor effects of cannabinoids. Neuropsychopharmacology *32*, 2249–2259.

Ciruela, F., Casadó, V., Mallol, J., Canela, E.I., Lluis, C., and Franco, R. (1995). Immunological identification of A1 adenosine receptors in brain cortex. J. Neurosci. Res. *42*, 818–828.

Ciruela, F., Escriche, M., Burgueno, J., Angulo, E., Casado, V., Soloviev, M.M., Canela, E.I., Mallol, J., Chan, W.Y., Lluis, C., et al. (2001). Metabotropic glutamate 1alpha and adenosine A1 receptors assemble into functionally interacting complexes. J. Biol. Chem. *276*, 18345–18351.

Csóka, B., Koscsó, B., Töro, G., Kókai, E., Virág, L., Németh, Z.H., Pacher, P., Bai, P., and Haskó, G. (2014). A2B adenosine receptors prevent insulin resistance by inhibiting adipose tissue inflammation via maintaining alternative macrophage activation. Diabetes *63*, 850–866.

Cui, X., Xiao, W., You, L., Zhang, F., Cao, X., Feng, J., Shen, D., Li, Y., Wang, Y., Ji, C., and Guo, X. (2019). Age-induced oxidative stress impairs adipogenesis and thermogenesis in brown fat. FEBS J. *286*, 2753–2768.

Cypess, A.M., Lehman, S., Williams, G., Tal, I., Rodman, D., Goldfine, A.B., Kuo, F.C., Palmer, E.L., Tseng, Y.H., Doria, A., et al. (2009). Identification and importance of brown adipose tissue in adult humans. N. Engl. J. Med. *360*, 1509–1517.

Cypess, A.M., White, A.P., Vernochet, C., Schulz, T.J., Xue, R., Sass, C.A., Huang, T.L., Roberts-Toler, C., Weiner, L.S., Sze, C., et al. (2013). Anatomical localization, gene expression profiling and functional characterization of adult human neck brown fat. Nat. Med. *19*, 635–639.

Cypess, A.M., Weiner, L.S., Roberts-Toler, C., Franquet Elía, E., Kessler, S.H., Kahn, P.A., English, J., Chatman, K., Trauger, S.A., Doria, A., and Kolodny, G.M. (2015). Activation of human brown adipose tissue by a β3-adrenergic receptor agonist. Cell Metab. *21*, 33–38.

Deacon, R.M. (2013). Measuring the strength of mice. J. Vis. Exp.

Dong, J., Dong, Y., Dong, Y., Chen, F., Mitch, W.E., and Zhang, L. (2016). Inhibition of myostatin in mice improves insulin sensitivity via irisin-mediated cross talk between muscle and adipose tissues. Int. J. Obes. *40*, 434–442.

Dumont, N.A., Bentzinger, C.F., Sincennes, M.C., and Rudnicki, M.A. (2015). Satellite cells and skeletal muscle regeneration. Compr. Physiol. *5*, 1027–1059.

Eckle, T., Krahn, T., Grenz, A., Köhler, D., Mittelbronn, M., Ledent, C., Jacobson, M.A., Osswald, H., Thompson, L.F., Unertl, K., and Eltzschig, H.K. (2007). Cardioprotection by ecto-5′-nucleotidase (CD73) and A2B adenosine receptors. Circulation *115*, 1581–1590.

Elfellah, M.S., Dalling, R., Kantola, I.M., and Reid, J.L. (1989). Beta-adrenoceptors and human skeletal muscle characterisation of receptor subtype and effect of age. Br. J. Clin. Pharmacol. *27*, 31–38.

Enerbäck, S. (2010). Human brown adipose tissue. Cell Metab. *11*, 248–252.

Ferraro, E., Pin, F., Gorini, S., Pontecorvo, L., Ferri, A., Mollace, V., Costelli, P., and Rosano, G. (2016). Improvement of skeletal muscle performance in ageing by the metabolic modulator Trimetazidine. J. Cachexia Sarcopenia Muscle *7*, 449–457.

Fleg, J.L., Morrell, C.H., Bos, A.G., Brant, L.J., Talbot, L.A., Wright, J.G., and Lakatta, E.G. (2005). Accelerated longitudinal decline of aerobic capacity in healthy older adults. Circulation *112*, 674–682.

Ford, G.A., Hoffman, B.B., Vestal, R.E., and Blaschke, T.F. (1992). Age-related changes in adenosine and beta-adrenoceptor responsiveness of vascular smooth muscle in man. Br. J. Clin. Pharmacol. *33*, 83–87.

Ford, G.A., Dachman, W.D., Blaschke, T.F., and Hoffman, B.B. (1995). Effect of aging on beta 2-adrenergic receptor-stimulated flux of K+, PO4, FFA, and glycerol in human forearms. J. Appl. Physiol. *78*, 172–178.

Fredholm, B.B., IJzerman, A.P., Jacobson, K.A., Klotz, K.N., and Linden, J. (2001). International Union of Pharmacology. XXV. Nomenclature and classification of adenosine receptors. Pharmacol. Rev. *53*, 527–552.

Fredholm, B.B., IJzerman, A.P., Jacobson, K.A., Linden, J., and Müller, C.E. (2011). International Union of Basic and Clinical Pharmacology. LXXXI. Nomenclature and classification of adenosine receptors–an update. Pharmacol. Rev. *63*, 1–34.

Fuenzalida, J., Galaz, P., Araya, K.A., Slater, P.G., Blanco, E.H., Campusano, J.M., Ciruela, F., and Gysling, K. (2014). Dopamine D1 and corticotrophin-releasing hormone type-2α receptors assemble into functionally interacting complexes in living cells. Br. J. Pharmacol. *171*, 5650–5664.

García-Nafría, J., Lee, Y., Bai, X., Carpenter, B., and Tate, C.G. (2018). Cryo-EM structure of the adenosine A_{2A} receptor coupled to an engineered heterotrimeric G protein. eLife *7*, e35946.

García-Prat, L., and Muñoz-Cánoves, P. (2017). Aging, metabolism and stem cells: spotlight on muscle stem cells. Mol. Cell. Endocrinol. *445*, 109–117.

Gary, R.K., and Kindell, S.M. (2005). Quantitative assay of senescence-associated beta-galactosidase activity in mammalian cell extracts. Anal Biochem. *343*, 329–334.

Ginés, S., Hillion, J., Torvinen, M., Le Crom, S., Casadó, V., Canela, E.I., Rondin, S., Lew, J.Y., Watson, S., Zoli, M., et al. (2000). Dopamine D1 and adenosine A1 receptors form functionally interacting heteromeric complexes. Proc. Natl. Acad. Sci. USA *97*, 8606–8611.

Gnad, T., Scheibler, S., von Kügelgen, I., Scheele, C., Kilić, A., Glöde, A., Hoffmann, L.S., Reverte-Salisa, L., Horn, P., Mutlu, S., et al. (2014). Adenosine activates brown adipose tissue and recruits beige adipocytes via A2A receptors. Nature *516*, 395–399.

Gouspillou, G., Bourdel-Marchasson, I., Rouland, R., Calmettes, G., Biran, M., Deschodt-Arsac, V., Miraux, S., Thiaudiere, E., Pasdois, P., Detaille, D., et al. (2014). Mitochondrial energetics is impaired in vivo in aged skeletal muscle. Aging Cell *13*, 39–48.

Guiu-Jurado, E., Unthan, M., Böhler, N., Kern, M., Landgraf, K., Dietrich, A., Schleinitz, D., Ruschke, K., Klöting, N., Faßhauer, M., et al. (2016). Bone morphogenetic protein 2 (BMP2) may contribute to partition of energy storage into visceral and subcutaneous fat depots. Obesity (Silver Spring) *24*, 2092–2100.

Haas, B., Mayer, P., Jennissen, K., Scholz, D., Berriel Diaz, M., Bloch, W., Herzig, S., Fässler, R., and Pfeifer, A. (2009). Protein kinase G controls brown fat cell differentiation and mitochondrial biogenesis. Sci. Signal. *2*, ra78.

Hauser, A.S., Attwood, M.M., Rask-Andersen, M., Schiöth, H.B., and Gloriam, D.E. (2017). Trends in GPCR drug discovery: new agents, targets and indications. Nat. Rev. Drug Discov. *16*, 829–842.

Heaton, J.M. (1972). The distribution of brown adipose tissue in the human. J. Anat. *112*, 35–39.

Hellsten, Y., Maclean, D., Rådegran, G., Saltin, B., and Bangsbo, J. (1998). Adenosine concentrations in the interstitium of resting and contracting human skeletal muscle. Circulation *98*, 6–8.

Hinz, S., Navarro, G., Borroto-Escuela, D., Seibt, B.F., Ammon, Y.C., de Filippo, E., Danish, A., Lacher, S.K., Červinková, B., Rafehi, M., et al. (2018). Adenosine A_{2A} receptor ligand recognition and signaling is blocked by A_{2B} receptors. Oncotarget *9*, 13593–13611.

Hua, X., Chason, K.D., Jania, C., Acosta, T., Ledent, C., and Tilley, S.L. (2013). Gs-coupled adenosine receptors differentially limit antigen-induced mast cell activation. J. Pharmacol. Exp. Ther. *344*, 426–435.

Inglés, M., Gambini, J., Carnicero, J.A., García-García, F.J., Rodríguez-Mañas, L., Olaso-González, G., Dromant, M., Borrás, C., and Viña, J. (2014). Oxidative stress is related to frailty, not to age or sex, in a geriatric population: lipid and protein oxidation as biomarkers of frailty. J. Am. Geriatr. Soc. *62*, 1324–1328.

Jespersen, N.Z., Larsen, T.J., Peijs, L., Daugaard, S., Homøe, P., Loft, A., de Jong, J., Mathur, N., Cannon, B., Nedergaard, J., et al. (2013). A classical brown adipose tissue mRNA signature partly overlaps with brite in the supraclavicular region of adult humans. Cell Metab. *17*, 798–805.

Johansson, S.M., Lindgren, E., Yang, J.N., Herling, A.W., and Fredholm, B.B. (2008). Adenosine A1 receptors regulate lipolysis and lipogenesis in mouse adipose tissue-interactions with insulin. Eur. J. Pharmacol. *597*, 92–101.

Johnston-Cox, H., Koupenova, M., Yang, D., Corkey, B., Gokce, N., Farb, M.G., LeBrasseur, N., and Ravid, K. (2012). The A2b adenosine receptor modulates glucose homeostasis and obesity. PLoS ONE *7*, e40584.

Jura, M., and Kozak, L.P. (2016). Obesity and related consequences to ageing. Age (Dordr.) *38*, 23.

Kajimura, S., Spiegelman, B.M., and Seale, P. (2015). Brown and beige fat: physiological roles beyond heat generation. Cell Metab. *22*, 546–559.

Kalinkovich, A., and Livshits, G. (2017). Sarcopenic obesity or obese sarcopenia: a cross talk between age-associated adipose tissue and skeletal muscle inflammation as a main mechanism of the pathogenesis. Ageing Res. Rev. *35*, 200–221.

Kendall, M.J., Woods, K.L., Wilkins, M.R., and Worthington, D.J. (1982). Responsiveness to beta-adrenergic receptor stimulation: the effects of age are cardioselective. Br. J. Clin. Pharmacol. *14*, 821–826.

Keyes, W.M., Wu, Y., Vogel, H., Guo, X., Lowe, S.W., and Mills, A.A. (2005). p63 deficiency activates a program of cellular senescence and leads to accelerated aging. Genes Dev. *19*, 1986–1999.

Kong, X., Yao, T., Zhou, P., Kazak, L., Tenen, D., Lyubetskaya, A., Dawes, B.A., Tsai, L., Kahn, B.B., Spiegelman, B.M., et al. (2018). Brown adipose tissue controls skeletal muscle function via the secretion of myostatin. Cell Metab. *28*, 631–643.e3.

Lahesmaa, M., Oikonen, V., Helin, S., Luoto, P., U Din, M., Pfeifer, A., Nuutila, P., and Virtanen, K.A. (2019). Regulation of human brown adipose tissue by adenosine and A_{2A} receptors - studies with [^{15}O]H_2O and [^{11}C]TMSX PET/CT. Eur. J. Nucl. Med. Mol. Imaging *46*, 743–750.

Lavoie, C., Mercier, J.F., Salahpour, A., Umapathy, D., Breit, A., Villeneuve, L.R., Zhu, W.Z., Xiao, R.P., Lakatta, E.G., Bouvier, M., and Hébert, T.E. (2002). Beta 1/beta 2-adrenergic receptor heterodimerization regulates beta 2-adrenergic receptor internalization and ERK signaling efficacy. J. Biol. Chem. *277*, 35402–35410.

Lidell, M.E., Betz, M.J., Dahlqvist Leinhard, O., Heglind, M., Elander, L., Slawik, M., Mussack, T., Nilsson, D., Romu, T., Nuutila, P., et al. (2013). Evidence for two types of brown adipose tissue in humans. Nat. Med. *19*, 631–634.

Lynge, J., and Hellsten, Y. (2000). Distribution of adenosine A1, A2A and A2B receptors in human skeletal muscle. Acta Physiol. Scand. *169*, 283–290.

Ma, X., Xu, L., Gavrilova, O., and Mueller, E. (2014). Role of forkhead box protein A3 in age-associated metabolic decline. Proc. Natl. Acad. Sci. USA *111*, 14289–14294.

Manglik, A., Kruse, A.C., Kobilka, T.S., Thian, F.S., Mathiesen, J.M., Sunahara, R.K., Pardo, L., Weis, W.I., Kobilka, B.K., and Granier, S. (2012). Crystal structure of the μ-opioid receptor bound to a morphinan antagonist. Nature *485*, 321–326.

Martí-Renom, M.A., Stuart, A.C., Fiser, A., Sánchez, R., Melo, F., and Sali, A. (2000). Comparative protein structure modeling of genes and genomes. Annu Rev Biophys Biomol Struct. *29*, 291–325.

Marzani, B., Felzani, G., Bellomo, R.G., Vecchiet, J., and Marzatico, F. (2005). Human muscle aging: ROS-mediated alterations in rectus abdominis and vastus lateralis muscles. Exp. Gerontol. *40*, 959–965.

Mashili, F.L., Austin, R.L., Deshmukh, A.S., Fritz, T., Caidahl, K., Bergdahl, K., Zierath, J.R., Chibalin, A.V., Moller, D.E., Kharitonenkov, A., and Krook, A. (2011). Direct effects of FGF21 on glucose uptake in human skeletal muscle: implications for type 2 diabetes and obesity. Diabetes Metab. Res. Rev. *27*, 286–297.

Masoro, E.J. (2005). Overview of caloric restriction and ageing. Mech. Ageing Dev. *126*, 913–922.

McGregor, R.A., Cameron-Smith, D., and Poppitt, S.D. (2014). It is not just muscle mass: a review of muscle quality, composition and metabolism during ageing as determinants of muscle function and mobility in later life. Longev. Healthspan *3*, 9.

Moore, N.G., Pegg, G.G., and Sillence, M.N. (1994). Anabolic effects of the beta 2-adrenoceptor agonist salmeterol are dependent on route of administration. Am. J. Physiol. *267*, E475–E484.

Moriyama, K., and Sitkovsky, M.V. (2010). Adenosine A2A receptor is involved in cell surface expression of A2B receptor. J. Biol. Chem. *285*, 39271–39288.

Motohashi, N., Asakura, Y., and Asakura, A. (2014). Isolation, culture, and transplantation of muscle satellite cells. J. Vis. Exp.

Nedergaard, J., Bengtsson, T., and Cannon, B. (2011). New powers of brown fat: fighting the metabolic syndrome. Cell Metab. *13*, 238–240.

Newman, A.B., Kupelian, V., Visser, M., Simonsick, E.M., Goodpaster, B.H., Kritchevsky, S.B., Tylavsky, F.A., Rubin, S.M., and Harris, T.B. (2006). Strength, but not muscle mass, is associated with mortality in the health, aging and body composition study cohort. J. Gerontol. A Biol. Sci. Med. Sci. *61*, 72–77.

Nicholson, T., Church, C., Baker, D.J., and Jones, S.W. (2018). The role of adipokines in skeletal muscle inflammation and insulin sensitivity. J. Inflamm. (Lond.) *15*, 9.

Orava, J., Nuutila, P., Lidell, M.E., Oikonen, V., Noponen, T., Viljanen, T., Scheinin, M., Taittonen, M., Niemi, T., Enerbäck, S., and Virtanen, K.A. (2011). Different metabolic responses of human brown adipose tissue to activation by cold and insulin. Cell Metab. *14*, 272–279.

Patlak, C.S., and Blasberg, R.G. (1985). Graphical evaluation of blood-to-brain transfer constants from multiple-time uptake data. Generalizations. J. Cereb. Blood Flow Metab. *5*, 584–590.

Pedersen, B.K., and Febbraio, M.A. (2012). Muscles, exercise and obesity: skeletal muscle as a secretory organ. Nat. Rev. Endocrinol. *8*, 457–465.

Peng, Y., McCorvy, J.D., Harpsøe, K., Lansu, K., Yuan, S., Popov, P., Qu, L., Pu, M., Che, T., Nikolajsen, L.F., et al. (2018). 5-HT_{2C} receptor structures reveal the structural basis of GPCR polypharmacology. Cell *172*, 719–730.e14.

Pfeifer, A., and Hoffmann, L.S. (2015). Brown, beige, and white: the new color code of fat and its pharmacological implications. Annu. Rev. Pharmacol. Toxicol. *55*, 207–227.

Ralevic, V., and Burnstock, G. (1998). Receptors for purines and pyrimidines. Pharmacol. Rev. *50*, 413–492.

Rantanen, T., Guralnik, J.M., Foley, D., Masaki, K., Leveille, S., Curb, J.D., and White, L. (1999). Midlife hand grip strength as a predictor of old age disability. JAMA *281*, 558–560.

Richter, E.A., and Hargreaves, M. (2013). Exercise, GLUT4, and skeletal muscle glucose uptake. Physiol. Rev. *93*, 993–1017.

Roatta, S., and Farina, D. (2010). Sympathetic actions on the skeletal muscle. Exerc. Sport Sci. Rev. *38*, 31–35.

Rodriguez, A.M., Pisani, D., Dechesne, C.A., Turc-Carel, C., Kurzenne, J.Y., Wdziekonski, B., Villageois, A., Bagnis, C., Breittmayer, J.P., Groux, H., et al. (2005). Transplantation of a multipotent cell population from human adipose tissue induces dystrophin expression in the immunocompetent mdx mouse. J. Exp. Med. *201*, 1397–1405.

Rosenwald, M., and Wolfrum, C. (2014). The origin and definition of brite versus white and classical brown adipocytes. Adipocyte *3*, 4–9.

Ruan, C.C., Kong, L.R., Chen, X.H., Ma, Y., Pan, X.X., Zhang, Z.B., and Gao, P.J. (2018). A_{2A} receptor activation attenuates hypertensive cardiac remodeling via promoting brown adipose tissue-derived FGF21. Cell Metab. *28*, 476–489.e5.

Ryzhov, S., Zaynagetdinov, R., Goldstein, A.E., Novitskiy, S.V., Dikov, M.M., Blackburn, M.R., Biaggioni, I., and Feoktistov, I. (2008). Effect of A2B adenosine receptor gene ablation on proinflammatory adenosine signaling in mast cells. J. Immunol. *180*, 7212–7220.

Sayer, A.A., Syddall, H., Martin, H., Patel, H., Baylis, D., and Cooper, C. (2008). The developmental origins of sarcopenia. J. Nutr. Health Aging *12*, 427–432.

Schiaffino, S., and Reggiani, C. (2011). Fiber types in mammalian skeletal muscles. Physiol. Rev. *91*, 1447–1531.

Shimizu, I., Aprahamian, T., Kikuchi, R., Shimizu, A., Papanicolaou, K.N., MacLauchlan, S., Maruyama, S., and Walsh, K. (2014). Vascular rarefaction mediates whitening of brown fat in obesity. J. Clin. Invest. *124*, 2099–2112.

Shinoda, K., Luijten, I.H., Hasegawa, Y., Hong, H., Sonne, S.B., Kim, M., Xue, R., Chondronikola, M., Cypess, A.M., Tseng, Y.H., et al. (2015). Genetic and functional characterization of clonally derived adult human brown adipocytes. Nat. Med. *21*, 389–394.

Short, K.R., Bigelow, M.L., Kahl, J., Singh, R., Coenen-Schimke, J., Raghavakaimal, S., and Nair, K.S. (2005). Decline in skeletal muscle mitochondrial function with aging in humans. Proc. Natl. Acad. Sci. USA *102*, 5618–5623.

Sousa-Victor, P., Gutarra, S., García-Prat, L., Rodriguez-Ubreva, J., Ortet, L., Ruiz-Bonilla, V., Jardí, M., Ballestar, E., González, S., Serrano, A.L., et al. (2014). Geriatric muscle stem cells switch reversible quiescence into senescence. Nature *506*, 316–321.

Stanford, K.I., and Goodyear, L.J. (2016). Exercise regulation of adipose tissue. Adipocyte *5*, 153–162.

Sui, W., Li, H., Yang, Y., Jing, X., Xue, F., Cheng, J., Dong, M., Zhang, M., Pan, H., Chen, Y., et al. (2019). Bladder drug mirabegron exacerbates atherosclerosis through activation of brown fat-mediated lipolysis. Proc. Natl. Acad. Sci. USA *116*, 10937–10942.

Takeshita, H., Yamamoto, K., Nozato, S., Inagaki, T., Tsuchimochi, H., Shirai, M., Yamamoto, R., Imaizumi, Y., Hongyo, K., Yokoyama, S., et al. (2017). Modified forelimb grip strength test detects aging-associated physiological decline in skeletal muscle function in male mice. Sci. Rep. *7*, 42323.

Trayhurn, P., Drevon, C.A., and Eckel, J. (2011). Secreted proteins from adipose tissue and skeletal muscle - adipokines, myokines and adipose/muscle cross-talk. Arch. Physiol. Biochem. *117*, 47–56.

Ussar, S., Lee, K.Y., Dankel, S.N., Boucher, J., Haering, M.F., Kleinridders, A., Thomou, T., Xue, R., Macotela, Y., Cypess, A.M., et al. (2014). ASC-1, PAT2, and P2RX5 are cell surface markers for white, beige, and brown adipocytes. Sci. Transl. Med. *6*, 247ra103.

van Marken Lichtenbelt, W.D., Vanhommerig, J.W., Smulders, N.M., Drossaerts, J.M., Kemerink, G.J., Bouvy, N.D., Schrauwen, P., and Teule, G.J. (2009). Cold-activated brown adipose tissue in healthy men. N. Engl. J. Med. *360*, 1500–1508.

Villarroya, F., Cereijo, R., Villarroya, J., and Giralt, M. (2017). Brown adipose tissue as a secretory organ. Nat. Rev. Endocrinol. *13*, 26–35.

Virtanen, K.A., Lidell, M.E., Orava, J., Heglind, M., Westergren, R., Niemi, T., Taittonen, M., Laine, J., Savisto, N.J., Enerbäck, S., and Nuutila, P. (2009). Functional brown adipose tissue in healthy adults. N. Engl. J. Med. *360*, 1518–1525.

Weinert, T., Olieric, N., Cheng, R., Brünle, S., James, D., Ozerov, D., Gashi, D., Vera, L., Marsh, M., Jaeger, K., et al. (2017). Serial millisecond crystallography for routine room-temperature structure determination at synchrotrons. Nat. Commun. *8*, 542.

Wu, J., Boström, P., Sparks, L.M., Ye, L., Choi, J.H., Giang, A.H., Khandekar, M., Virtanen, K.A., Nuutila, P., Schaart, G., et al. (2012). Beige adipocytes are a distinct type of thermogenic fat cell in mouse and human. Cell *150*, 366–376.

Zamboni, M., Mazzali, G., Fantin, F., Rossi, A., and Di Francesco, V. (2008). Sarcopenic obesity: a new category of obesity in the elderly. Nutr. Metab. Cardiovasc. Dis. *18*, 388–395.

Zhang, X., Wang, X., Yin, H., Zhang, L., Feng, A., Zhang, Q.-X., Lin, Y., Bao, B., Hernandez, L.L., Shi, G.-P., and Liu, J. (2019). Functional inactivation of mast cells enhances subcutaneous adipose tissue browning in mice. Cell Rep. *28*, 792–803.e4.

Zierath, J.R., and Wallberg-Henriksson, H. (2015). Looking ahead perspective: where will the future of exercise biology take us? Cell Metab. *22*, 25–30.

STAR★METHODS

KEY RESOURCES TABLE

REAGENT or RESOURCE	SOURCE	IDENTIFIER
Antibodies		
Rabbit polyclonal anti-UCP-1	ThermoFisher	Custom made
Mouse monoclonal anti-AdoR A2A (7F6-G5-A2)	Santa Cruz	#sc-33261
Goat polyclonal anti AdoR A2B (R-20)	Santa Cruz	#sc-7507
Goat polyclonal anti AdoR A1 (C-19)	Santa Cruz	#sc-7500
Mouse monoclonal anti-Actin (AC-74)	SigmaAldrich	#A2228; RRID: AB_476743
Mouse monoclonal anti CD71 (3B8 2A1)	Santa Cruz	sc-32272; RRID: AB_627167
Myosin Heavy Chain 1	DSHB	BA-F8-c
Myosin Heavy Chain 2A	DSHB	BF-F3-c
Myosin Heavy Chain 2B	DSHB	SC-71-c
Bacterial and Virus Strains		
Lentivirus shControl	This study	N/A
Lentivirus shA1	This study	N/A
Biological Samples		
Human BAT biopsies	Turku PET Centre, Finland	N/A
Human WAT sample collection	University of Leipzig, Germany	approval number: 017-12-23012012
Human SKM samples	University of Cologne and Düsseldorf, Germany	N/A
Chemicals, Peptides, and Recombinant Proteins		
Bay 60-6583	Tocris	# 4472
PSB 603	Tocris	# 3198
CGS 21680	Tocris	# 1063
A2A TM4 RRRQRRKKRGYAKGIIAICWVLSFAIGLTPMLGW	Biomatik	Custom made
A2A TM5 MNYMVYFNFFACVLVPLLLMLGVYL YGRKKRRQRRR	Biomatik	Custom made
A2A TM6 RRRQRRKKRGYLAIIVGLFALCWLPLHIINCFTFF	Biomatik	Custom made
A2B TM4 RRRQRRKKRGYARGVIAVLWVLAFGIGLTPFLGW	Biomatik	Custom made
A2B TM5 MSYMVYFNFFGCVLPPLLIMLVIYIYGRKKRRQRRR	Biomatik	Custom made
A2B TM6 RRRQRRKKRGYLAMIVGIFALCWLPVHAVNCVTLF	Biomatik	Custom made
Critical Commercial Assays		
DuoLink PLA Kit	SigmaAldrich	N/A
Piccolo General Chemistry 13	Hitado	114-400-0029
Piccolo Lipid Plus	Hitado	114-400-0030
Piccolo Metlyte 8	Hitado	114-400-0023
Piccolo Basic Metabolic Plus	Hitado	114-400-0031
4-HNE assay	Abcam	ab238538
Experimental Models: Cell Lines		
C2C12	ATCC	CRL-1772
Human skeletal muscle cells	Promo Cell	C-12530
Human brown adipocytes	Jespersen et al., 2013	N/A
hMADS	Rodriguez et al., 2005	N/A
Experimental Models: Organisms/Strains		
Adenosine A2B receptor knockout mouse	Eckle et al., 2007	N/A
HSA-Cre	Jackson Laboratories	Strain 025750

(*Continued on next page*)

Continued		
REAGENT or RESOURCE	SOURCE	IDENTIFIER
Adipoq-Cre	Jackson Laboratories	Strain 010803
A2Bfloxed	Aherne et al., 2015	N/A
Oligonucleotides		
Gs-coupled GPCR primer		
A2B 5′-gtggaacagtaaagacagtg; 5′-ccatgaagattttgatgtag	This study	N/A
Adrb3 5′-gagactacagaccataacc; 5′-atgctagcagttacacag	This study	N/A
Drd1 5′-tcaatcagaaagttccttta; 5′-ggcattaaaagcataaataa	This study	N/A
Mc4r 5′-tggacaggtatttcactatc; 5′-gaacatgtggacatagagag	This study	N/A
Tshr 5′-accaggaatatgaagaagat; 5′-acacaccgtgtagtcatagt	This study	N/A
Recombinant DNA		
A2Amut (F257A; F258A)	This study	N/A
A2Bmut (L258A; F259A)	This study	N/A
Software and Algorithms		
Modeler 9.18 software	Martí-Renom et al., 2000	https://salilab.org/modeller/
Graph pad prism V7	Graph pad software	https://graphpad.com

RESOURCE AVAILABILITY

Lead Contact

Further information and requests for resources and reagents should be directed to and will be fulfilled by the Lead Contact, Alexander Pfeifer (alexander.pfeifer@uni-bonn.de).

Materials Availability

This study generated adipose-tissue and skeletal muscle-specific A2B null mice. Availability of A2B floxed mice is restricted due to a MTA.

Data and Code Availability

This study did not generate/analyze datasets or codes. The data that support the findings of this study are available from the corresponding author upon reasonable request.

EXPERIMENTAL MODEL AND SUBJECT DETAILS

Mice

WT male C57BL/6 mice at indicated ages were purchased from Janvier.

A2B−/− mice (C57BL/6 background) were provided by M. Idzko, Freiburg, Germany. Only male A2B−/− and A2B+/+ littermates were analyzed.

ATA2B-KO (A2Bfloxed/floxed;AdipoCre+) and Con-A2B (A2Bfloxed/floxed;AdipoCre-) mice were generated by breeding A2Bfloxed/floxed mice (generated by Holger K. Eltzschig) with Adiponectin-Cre (Jackson Laboratories) mice to produce A2Bfloxed;AdipoCre+ heterozygous mice. Heterozygous mice were bred with A2Bfloxed/floxed. Male littermates were randomly assigned to experimental groups. A2Bfloxed/floxed as well as AdipoCre mice have a C57BL/6 background.

SKMA2B-KO (A2Bfloxed/floxed;HSA-Cre+) and Con-A2B (A2Bfloxed/floxed;HSA-Cre-) mice were generated by breeding A2Bfloxed/floxed mice with HSA-Cre (Jackson Laboratories; strain 025750; C57BL/6 background) to produce A2Bfloxed;HAS-Cre+ heterozygous mice. Heterozygous mice were bred with A2Bfloxed/floxed. Tamoxifen (100 mg/kg) was injected once daily for five consecutive days. Male mice were analyzed at 2 month (young) or 16 months (old/aged) of age.

HFD (60% energy from fat) and control diet was purchased from Ssniff (HFD: EF D12492, #E15741-347; control diet: EF D12450B, #E15748-047). Mice were maintained on a daily cycle of 12 h light (0600 to 1800) and 12 h darkness (1800 to 0600), at 23 ± 1°C, and were allowed free access to chow and water.

For the HFD study, 8-week-old male mice were injected *i.p.* once daily with A2B agonist Bay 60-6583 (1 mg/kg) for twelve weeks. Health status was checked daily and included measuring of body weight, observation of unprovoked behavior and responses to external stimuli, as well as assessment of physical appearance.

For muscle analysis/sarcopenia, male mice of indicated ages were injected once daily *i.p.* for four weeks with 1mg/kg Bay 60-6583.

Sample sizes for all *in vivo* experiments are given in the Figure legends.

All animal studies were performed in accordance with national guidelines and were approved by the Landesamt für Natur, Umwelt und Verbraucherschutz, Nordrhein-Westfalen, Germany.

Human Studies

Human BAT Studies (Turku, Finland)

Human PET imaging studies and human biopsy procedures were performed at the Turku PET Centre, Finland. The subjects who signed separate informed consent for biopsies were included to this study and altogether they are part of two separate imaging study cohorts. The study protocol was reviewed and approved by the ethics committee of the Hospital District of Southwest Finland and was conducted according to the principles of the Declaration of Helsinki. Exclusion criteria included regular use of any medication, use of tobacco or nicotine products, and any significant chronic disease such as asthma, diabetes, thyroid disease or cardiovascular disease. The age of the subjects ranged from 18 to 54 years and all subjects were male. Therefore, the influence of sex cannot be reported.

Human WAT Sample Collection (Leipzig, Germany)

The human sub-study was approved by the ethics committee of the University of Leipzig (approval number: 017-12-23012012) and all subjects gave written informed consent before taking part in the study. Paired samples of abdominal, omental visceral and subcutaneous adipose tissue were obtained from 405 Caucasian men (n = 119) and women (n = 286), who underwent open abdominal surgery as described previously (Guiu-Jurado et al., 2016). The age ranged from 16 to 93 years and BMI from 19 to 76 kg/m^2. Adipose tissue was immediately frozen in liquid nitrogen and stored at −80°C. RNA was extracted from adipose tissue by using RNeasy Lipid Tissue Mini Kit (QIAGEN). Quantity and integrity of RNA was monitored with NanoVue plus Spectrophotometer (GE Healthcare). 1 μg total RNA from each sample was reverse-transcribed with standard reagents (Life Technologies) and cDNA was analyzed with TaqMan probe-based quantitative real-time polymerase chain reaction using QuantStudio 6 Flex Real-Time PCR System (Life Technologies). Human *A2B* expression was measured using the following probe: human A2B (Hs00386497_m1). Human *A2B* mRNA expression was calculated relative to the mRNA expression of hypoxanthine guanine phosphoribosyltransferase 1 (HPRT1) (Hs01003267_m1). We tested for a potential influence of sex on the significant correlations between A2B expression in subcutaneous WAT, BMI and body weight. After adjusting for sex, correlations between subcutaneous A2B and BMI (adjusted $r = -0.163$, $p < 0.001$) and between subcutaneous A2B and body weight (adjusted $r = -0.148$, $p < 0.01$) remained significant suggesting that sex does not affect the observed correlations.

Human SKM Biopsy Procedure and Sample Collection (Cologne/Düsseldorf, Germany)

Biopsies were obtained from the middle portion of the *M. vastus lateris* between the spina iliaca anterior superior and the lateral part of the patella. A local anesthetic injection (xylocaine) was set. A 2 cm incision was made through skin and fascia and tissue was gathered 2,5 cm below the fascia using the percutaneous needle biopsy technique. Muscle samples were freed from blood and non-muscle material, frozen in liquid nitrogen and stored at −80°C for further analysis. This study/biopsy acquisition was approved by the local ethics committees and all subjects gave written informed consent before taking part. For Cohort 1, the age of subjects ranged from 33 to 74 years and all subjects were male. Therefore, no influence of sex can be reported. For Cohort 2, biopsies were obtained from 7 male and 5 female donors with an age ranging from 39 to 61 years. There was no influence of sex on the results of our analysis.

Subject information for all human studies can be found in Tables S6–S9.

Cells

Primary Human and Murine Adipocyte Culture

SVF cells from interscapular BAT from newborn mice of mixed sex were isolated and differentiated as described previously (Gnad et al., 2014) using collagenase digestion buffer [123 mM Na^+, 5 mM K+, 1.3 mM Ca^{2+}, 131 mM Cl−, 5 mM glucose, 1.5% (w/v) bovine serum albumin (BSA), 100 mM HEPES, 0.2% (w/v) collagenase type II (pH 7.4)]. After 30 min incubation at 37°C with regular shaking, tissue remains were removed by filtration using a 100-μm nylon mesh and cells were placed on ice for 30 min. The infranatant with the preadipocytes was filtered through a 30-μm nylon mesh and centrifuged at 700 x g for 10 min. The pellet was re-suspended and cells expanded in Dulbecco's modified Eagle's medium (DMEM) supplemented with 10% fetal bovine serum (FBS), 100 IU penicillin, streptomycin (100 μg/mL) (P/S), 4 nM insulin, 4 nM triiodothyronine, 100 mM HEPES, and sodium ascorbate (25 μg/mL), and grown at 37°C and 5% CO_2. For differentiation, cells were cultured in DMEM (GIBCO, #61965) containing 100 IU/mL penicillin, 100 μg/mL streptomycin, 10% FBS (heat-inactivated), 20 nM insulin as well as 1 nM Trijodothyronin-Na at 37°C and 5% CO_2. For induction, 1 μM Dexamethasone and 0.5 mM IBMX were added to this differentiation medium once for 2 days.

Primary human BA were isolated as described (Jespersen et al., 2013) and cultured in 60mm culture dishes containing DMEM/F12, 10% FBS, 1% Penicillin/Streptomycin (all from Invitrogen) and 1nM acidic FGF-1 (ImmunoTools). Cells were incubated at 37°C with 5% CO_2. Adipocytes were induced two days after full confluence with DMEM/F12 containing 1% Penicillin/Streptomycin, 0.1 μM dexamethasone (Sigma-Aldrich), 100 nM insulin, 200 nM rosiglitazone(Sigma-Aldrich), 540 μM isobutylmethylxanthine (Sigma--Aldrich), 2 nM T3 (Sigma-Aldrich) and 10 μg/mL transferrin (Sigma-Aldrich). After three days of differentiation, isobutylmethylxanthine was removed from the cell culture media. The cell cultures were left to differentiate for an additional nine days. Data were obtained from cells of one male and one female donor.

hMADS cells were obtained from the stroma of human adipose tissue and differentiated as described previously described (Rodriguez et al., 2005). Briefly, 200 mg adipose tissue from the pubic region fat pad of a 4-month-old male donor was dissociated for 10 min in DMEM containing antibiotics (100 U/mL of penicillin and 100 g/mL of streptomycin), 2 mg/mL collagenase, and 20 mg/mL

bovine serum albumin. Then, the crude SVF was separated from the adipocyte fraction by low speed centrifugation (200 g, 10 min). The adipocyte fraction was discarded and cells from the pelleted SVF were seeded onto uncoated tissue culture plates (Greiner) at 1,000–3,500 cells/cm2 in low glucose DMEM (Invitrogen) supplemented with 10% heat-inactivated fetal bovine serum, 2.5 ng/mL FGF2 and antibiotics as described before. After reaching 70% confluence, adherent cells were dissociated (0.25% trypsin EDTA; Invitrogen) and re-seeded at 1,000–3,000 cells/cm2 for expansion. Cells were cultured at 37°C with 5% CO2. For differentiation, confluent cells were cultured in DMEM/Ham's F12 media (50:50 v/v) supplemented with 10 μg/mL transferrin, 100 μM ascorbic acid 2-sodium, 0.85 μM insulin, 20 nM sodium selenite, 0.2 nM triiodothyronine, 1 μM dexamethasone, 100 μM isobutyl-methylxanthine and 1 μM rosiglitazone. 3 d later, the medium was changed (dexamethasone and isobutyl-methylxanthine were omitted).

METHOD DETAILS

BAT [^{18}F]FDG-PET imaging

Healthy male subjects participated in [^{18}F]FDG -PET/MRI scans to quantify glucose uptake of BAT. Before the scans, the study subjects fasted overnight and avoided strenuous exercise for a minimum of 24 h. Imaging was performed during cold exposure using a 3T Philips Ingenuity TF PET/MR scanner (Philips Health Care). Prior to the PET scan the subject lay in a supine position between two cooling blankets (Blanketrol III, Cincinnati Sub-Zero) with chilled flowing water for two h. Blanket temperature was determined and adjusted individually to maintain a subjectively cold temperature but avoid muscle shivering (average temperature 16.2 degrees). Cooling was maintained during the PET scan with cool air conditioning and by placing iced gel packets on the upper body and legs. 150 MBq of [^{18}F]FDG was injected intravenously and a 40-min dynamic PET scan of the cervical region was performed (using frames 7 × 60 s, 6 × 300 s, 1 × 180 s). Eight consecutive modified 2-point Dixon sequences (mDixon) were used to provide anatomical reference in the whole-body area and for calculating signal fat fraction (SFF) maps. Image analysis was performed using Carimas 2.9 software (Turku PET Centre, Turku, Finland). Regions of interest were manually drawn on the fused PET/MR images in supraclavicular areas of adipose tissue, confirmed with MR SFF maps. Glucose uptake was quantified using the Patlak linearization model (Patlak and Blasberg, 1985). High BAT and low BAT groups were determined by the cold-induced BAT glucose uptake values, where high BAT subjects had a glucose uptake of $\leq$ 3.0 mmol/100 g/min, as previously described (Orava et al., 2011).

Human BAT Biopsy Procedures

Twelve subjects gave written informed consent for acquiring tissue biopsies from the supraclavicular neck region. Biopsies of BAT were taken by a plastic surgeon through one skin incision in standard operating room conditions. Anatomical location of BAT was verified with individual [^{18}F]FDG -PET/MR or [^{15}O]H_2O-PET/CT images. If the glucose uptake was low (as in the overweight subjects), the SSF MRI-images were used to localize BAT in the supraclavicular area. Using these images, the location of the BAT depot was determined by measuring its distance from the suprasternal notch and the surface of the skin. Using these coordinates, the biopsies were obtained by a plastic surgeon (Lahesmaa et al., 2019; Virtanen et al., 2009). After removal, samples were immediately snap-frozen into liquid nitrogen and stored in −70 degrees until analysis.

Skeletal Muscle Isolation and Force Measurement

Extensor digitorum longus (EDL) muscles from the hind limbs of mice were isolated tendon-to-tendon, immersed into an organ bath containing Krebs buffer (118 mM NaCl, 3.4 mM KCl, 0.8 mM MgSO4, 1.2 mM KH2PO4, 11.1 mM glucose, 25 mM NaHCo3, 2.5 mM CaCl2) and bubbled with carbogen at RT. Muscles were aligned between the clamp of a lever arm and the hook of a force transducer of a myograph (SI Instruments). Then, Muscles were stretched until a single pulse elicited maximum force during a twitch stimulation. Twitch stimulations were recorded (2 V, 1 ms) for 2 minutes and force was measured. Total muscle cross-sectional area was estimated by dividing the muscle mass by the product of the muscle length, muscle length to fiber length ratios (0.44 for EDL) and the density of mammalian muscle (1.06 mg/mm^3). Specific force was calculated as force/total cross sectional area (mN/mm2)

In Vivo Weight Lift

After 12-week CD or HFD with daily A2B ago treatment, mice underwent weight lifting assay as described (Deacon, 2013) to determine muscle strength. Mice lifted weight (chain links connected to steel wool) ranging from 15 g to 94 g.

Forelimb Grip Test

Mice were lowered over the grid keeping the torso horizontal and allowing only forepaws to attach to the grid. Then, mice were gently pulled back by the tail ensuring mice grid the top portion of the grid and the torso remain horizontal and record the maximal grip strength value. 3 forelimb grip strength measurements were performed per mouse.

Measurement of Endogenous Respiration

Skeletal muscle cells or tissue were treated as indicated 15 min before oxygraph measurements (Oxygraph 2K; Oroboros Instruments). Samples were transferred to the oxygraph chamber containing 2 mL incubation medium (0.5 mM EGTA, 3 mM MgCl2 6H2O, 60 mM K-lactobionate, 20 mM taurine, 10 mM KH2PO4, 20 mM HEPES, 110 mM sucrose and 1 g/l BSA, pH 7.1). *In vitro* respiration levels were recorded when reaching a steady state followed by addition of substrates (State 1: endogenous; state 2: ADP; state 3: succinate; state 4: oligomycin; uncoupled: FCCP). Respiration rates were normalized to total protein content

Glucose Uptake Assay

Glucose uptake was measured with murine and human SKM cells using glucose uptake kit from Abcam (#136956) according to manufacturer's instructions.

Beta-Hexosaminidase Release/Degranulation Assay

PMCs were re-suspended at concentration $2x10^6$ cells/mL in solution containing (mM): NaCl 130; KCl 5; CaCl2 1.4; MgCl2 1; glucose 5,6; HEPES 10, 0,1% Bovine Serum Albumine (Fraction V); pH 7.4 adjusted with NaOH. The cells were seeded in a V-bottom 96-well plate (100µl/well) and 25µl solution of corresponding agonists/antagonists was added. The PMCs were incubated 45 min at 37°C. After a short centrifugation step (1000 g for 5 min at 4°C) the cell lysates (solubilized with 1% Triton-X during 5 min at room temperature) and supernatants were incubated separately with 2 mM of a colorigenic substrate 4-Nitrophenyl N-acetyl-β-D-glucosaminide for 1 h at 37°C. The reaction was stopped by adding 200 mM glycine (pH 10.7 with NaOH). The absorbance (405nm) of the resulting probes was quantified using a NanoQuant infinite M200pro (Tecan, Switzerland) spectrophotometer. The percentage of β-hexosaminidase release was calculated as a ratio of absorbance of the supernatant to the total (sum of supernatant and lysate) β-hexosaminidase content.

Glycolysis

Glycolysis was measured with murine and human SKM cells using glucose uptake kit from Abcam (#197244) according to manufacturer's instructions.

Senescence-Associated Beta-Galactosidase Activity Assay

BAT and SKM were homogenized with lysis buffer containing 5 mM 3-[(3-cholamidopropyl)dimethylammonio]-1-propanesulfonate [CHAPS], 40 mM citric acid, 40 mM sodium phosphate, 0.5 mM benzamidine, and 0.2 5mM phenylmethanesulfonyl xuoride [PMSF], pH 6.0). Enzyme activity was then measured as described previously (Gary and Kindell, 2005) .

Lipolysis Assay

Differentiated adipocytes were washed twice with lipolysis medium (Life Technologies, DMEM21603) supplemented with 2% w/v fatty acid–free BSA (Sigma-Aldrich) followed by incubation with lipolysis medium containing indicated substances at 37°C and 5% CO_2 for two (murine) or four (human) h.

Cell culture media were collected, incubated 5 min at 37°C with free glycerol reagent (Sigma-Aldrich) and absorption was measured at 540 nm. Glycerol release was calculated with glycerol standard (Sigma-Aldrich) and normalized to protein content.

Immunoblot

Protein amount from all samples was quantified using Bradford assay followed by concentration normalization before western blot experiments. Western blot was carried out following standard procedures.

RNA Isolation and qPCR

Total RNA was isolated from cells or tissues using Trizol (Invitrogen). Reverse transcription was performed using ProtoScript II (NEB) qPCR was performed with SYBR-Green (Roche) using a HT7900 machine (Applied Biosystems). Expression levels were calculated as delta Ct values relative to house-keeping genes mHPRT (hypoxanthine guanine phosphoribosyl transferase) or hTBT (TATA-box binding protein) serving as control.

Bioluminescence Resonance Energy Transfer

HEK293T cells or adipocytes were transiently co-transfected with a constant amount of cDNA encoding A2A fused to RLuc and increasing amounts of cDNA encoding A2B-YFP. To quantify A2B-YFP expression, cells (20 µg protein) were distributed in 96-well microplates (black plates with a transparent bottom) and fluorescence was read in the Fluo Star Optima Fluorimeter using a 10 nm bandwidth excitation filter at 400 nm reading. Protein fluorescence expression was determined as fluorescence of the sample minus the fluorescence of cells expressing the BRET donor alone. For BRET measurements, the equivalent of 20 µg of cell suspension were distributed in 96-well microplates (Corning 3600, white plates) and 5 µM coelenterazine H (Molecular Probes) was added. After 1 min the readings were collected using a Mithras LB 940 (Berthold Technologies) that allows the integration of the signals detected in the short-wavelength filter at 485 nm and the long-wavelength filter at 530 nm. To quantify A2A-RLuc expression luminescence readings were performed after 10 min of adding 5 µM coelenterazine H.

Peptide Design

Peptides containing transmembrane regions of A2B andA2A fused to the YGRKKRRQRRRPQ sequence of the HIV-1 transactivation of transcription protein (tat), were purchased from Biomatik.

Pharmacological Activation of Energy Expenditure

8-week-old male C57BL/6 WT, ATA2B-KO or Con-A2B mice were injected subcutaneously with A2A agonist CGS21680 (1 mg/kg) five minutes before measurement. Oxygen consumption was measured for 120 s every 6 min with Phenomaster (TSE Systems). Time-course and relative increase (relative to respective t = 0) are shown.

Physiological Activation of Energy Expenditure

8-week-old male C57BL/6 WT were injected subcutaneously with PSB603 (1 mg/kg) and directly put into Phenomaster cages at 4°C. Animals were measured for 100 s every 5 min for 1 h.

PET/MRI of BAT Activation

PET/MRI (nanoScan PET-MRI, Mediso Medical Imageing Systems, Hungary) studies were performed on 8-week-old male C57BL\6 WT mice. Subcutaneous injection of vehicle, NE (1 mg/kg) or Bay 60-6583 (0.1 mg/kg) was performed one minute before *i.p.* injection of 14.7 ± 0.4 MBq of [^{18}F]FDG into conscious animals. Anesthesia was induced 10 min before start of the PET protocol. The PET/MRI scan was performed 60-75 min *p.i.* of [^{18}F]FDG followed by static data reconstruction (3D ordered-subset expectation maximization, 4 iterations, 6 subsets, MRI-based attenuation correction). As a measure of activity, the tracer accumulation was expressed as mean standardized uptake value (SUV).

Body Composition Analysis

Body composition was analyzed using a table Bruker Minispec.

Glucose Tolerance Test

Animals were fasted for 5 h. Eight μl/g body weight of glucose solution (2.5 g/mL) were injected *i.p.* and glucose was measured at indicated time points post injection. Tail vein was punctured and blood was analyzed with Accu Check (Aviva Nano) analyzer and dipsticks (Roche).

Thermography

Thermographic images were taken from newborn littermates at room temperature with an infrared camera (IC060, Trotec) and analyzed with IC-Report software 1.2 (Trotec).

Satellite Cell Isolation

Satellite cells were isolated from leg muscles of A2B+/+ and A2B−/− as well as from WT mice treated once daily with Bay 60-6583 (1mg/kg) for four weeks as described (Motohashi et al., 2014).

Immunohistochemistry and PLA

Five-micrometre paraffin-embedded BAT and WAT sections were blocked with 2.5% normal goat serum–PBST (phosphate-buffered saline + 0.1% Tween-20) for 1 h at room temperature. Primary antibody (UCP-1, 1:50) was applied overnight at 4°C. After washing three times with PBST, secondary antibody against rabbit (SignalStain Boost IHC, Cell Signaling) was applied for 1 h at room temperature and developed with DAB Kit (Vector Laboratories) according to the manufacturer's instructions. Standard hematoxylin and eosin (H&E) staining was performed on 5-μm paraffin-embedded BAT and WAT sections. PLA was performed with 10 μm BAT cryosections using DuoLink (Sigma-Aldrich) with A2B (C-20) and A2A (7F6-G5-A2) antibodies from Santa Cruz and Topro3 (ThermoFisher Scientic) as counter stain for nuclei.

Molecular Modeling

The A2A/A2B heterotetramer consists of two homodimers of the human A2A (Uniprot entry P29274) and A2B (UniProt: P29275) receptors. Each homodimer contains inactive and active, Gs-bound, protomers. The inactive A2A protomer was modeled from the A2A crystal structure (PDB: 5NM4) (Weinert et al., 2017) and the active A2A protomer was modeled from the structure of A2AR in complex with mini-Gs (PDB: 6GDG) (García-Nafría et al., 2018). The structures of inactive and active A2B protomers were modeled from the respective A2A structures (these receptors share 47% of sequence identity and 59% of sequence similarity) using Modeler 9.21. The globular α-helical domain of the α-subunit was modeled in the "closed" conformation. To identify the arrangement of A2A and A2B protomers in the heterotetramer, we used TAT-fused synthetic peptides. These experiments predicted the TM4/5 interface for homo- and TM5/6 interface for hetero-dimerization. The TM4/5 interfaces for both A2A and A2B homodimers were modeled as observed in the structure of the 5-HT2C receptor (PDB: 6BQG) (Peng et al., 2018), whereas the TM5/6 heteromeric interface was modeled as observed in the structure of the μ-opioid receptor (PDB: 4DKL) (Manglik et al., 2012).

Site-Directed Mutagenesis

Site-directed mutagenesis of F257A/F258A in A2A and L258A/F259A in A2B was performed with Q5-Kit (NEB). Primer were designed using NEBaseChanger Software (NEB).

QUANTIFICATION AND STATISTICAL ANALYSIS

To determine the group size necessary for sufficient statistical power, power analysis was performed with PS Power and Sample Size Calculation Software using preliminary data and all experiments were designed and powered to a minimum of 0.8 as calculated.

Normal distribution of data was tested using D'Agostino-Pearson omnibus test. *P* values below 0.05 were considered significant. Statistical analysis and data plotting was performed with GraphPad prism 7 software. Data are represented as scatter blots, bar graphs showing mean + SEM and individual data points or boxplots (with median) and whiskers (1.5x interquartile range), except of BRET data which are represented as mean ± SD; Please refer to Figure legends for description of sample sizes and statistical test performed.